J. Fluid Mech. (1996), *vol.* 326, *pp.* 91–123

Magnetohydrodynamic flow in a right-angle bend in a strong magnetic field

By R. STIEGLITZ[1], L. BARLEON[1], L. BÜHLER[1] AND S. MOLOKOV[2]

[1] JATF, Forschungszentrum Karlsruhe GmbH, Postfach 3640, D-76021 Germany

[2] Coventry University, MIS, Priory Street, Coventry CV1 5FB, UK

(Received 28 July 1995 and in revised form 17 May 1996)

The magnetohydrodynamic (MHD) flow through sharp 90° bends of rectangular cross-section, in which the flow turns from a direction almost perpendicular to the magnetic field to a direction almost aligned with the magnetic field, is investigated experimentally for high values of the Hartmann number M and of the interaction parameter N. The bend flow is characterized by strong three-dimensional effects causing a large pressure drop and large deformations in the velocity profile. Since such bends are basic elements of fusion reactors, the scaling laws of magnetohydrodynamic bends flows with the main flow parameters such as M and N as well as the sensitivity to small magnetic field inclinations are of major importance. The obtained experimental results are compared to those of an asymptotic theory.

In the case where one branch of the bend is perfectly aligned with the magnetic field good agreement between the results obtained by the asymptotic model and by the experiments was found at high $M \approx 8 \times 10^3$ and $N \approx 10^5$ for pressure as well as for electric potentials on the duct surface. At lower values of N a significant influence of inertia has been detected. The pressure drop due to inertial effects was found to scale with $N^{-1/3}$. The same $-1/3$-power dependency on N has been found in the vicinity of the bend for the electric potentials at walls aligned with the magnetic field. At walls with a significant normal component of the field an influence neither of the Hartmann number nor of the interaction parameter has been found. This suggests that the inertial part of the pressure drop arises from inertial side layers, whereas the core flow remains inertialess and inviscid. A variation of the Hartmann number is of negligible influence compared to inertia effects with respect to pressure drop and surface potential distribution. The viscous part of the pressure drop scales with $M^{-1/2}$.

Changes of the magnetic field orientation with respect to the bend lead in general to different flow patterns in the duct, because the electric current paths are changed. The inertia–electromagnetic interaction determines the magnitude of the inertial part of the pressure drop, which scales with $N^{-1/3}$ for any magnetic field orientation. The dependence of the pressure drop on M remains proportional to $M^{-1/2}$. With increasing M and N the measured data tend to those predicted by the asymptotic model. Local measurements within the liquid metal exhibit discrepancies with the model predictions for which no adequate explanation has been found. But they show that below a critical interaction parameter flow regions exist in which the flow is time dependent. These regions are highly localized, whereas the flow in the rest of the bend remains steady.

1. Introduction

Magnetohydrodynamic (MHD) flows in bends of rectangular cross-section in the plane of a strong uniform magnetic field have received considerable attention during the last few years. Such MHD flows have been studied theoretically by Moon & Walker (1990), Moon, Hua & Walker (1991), Hua & Walker (1991), Bühler (1993, 1995) and Molokov & Bühler (1994, 1995), and experimentally by Barleon *et al.* (1992, 1993*a*, *b*) and Reimann *et al.* (1994).

Apart from its practical importance in fusion blanket applications (Malang *et al.* 1988), the MHD bend flow is an interesting subject on its own right. It involves all the characteristic features of three-dimensional MHD flows in a strong magnetic field in their most clearly manifested form. These features are the formation of inertialess inviscid cores, and boundary and internal layers, some of which are able to carry a significant part of the volume flux in high-velocity jets.

Liquid-metal magnetohydrodynamic flows are controlled by the following four dimensionless parameters: the magnetic Reynolds number R_m, the interaction parameter N, the Hartmann number M and the wall conductance radio c:

$$R_m = \mu\sigma v_0 a; \quad N = \frac{\sigma a B_0^2}{\rho v_0}; \quad M = aB_0\left(\frac{\sigma}{\rho\nu}\right)^{1/2}; \quad c = \frac{\sigma_W t_W}{\sigma a}.$$

Here μ, σ, ρ and ν are the magnetic permeability, electrical conductivity, density and kinematic viscosity of the liquid metal; a is a characteristic length scale of a duct cross-section; σ_W and t_W are the electrical conductivity and the thickness of the duct walls; B_0 is the induction of the applied uniform magnetic field and v_0 is the average fluid velocity in the duct. The magnetic Reynolds number R_m is proportional to the ratio of the magnetic field induced by the electric currents to the applied field, which is assumed to be strong. For the type of application considered R_m is usually of the order of 10^{-2}, see Holroyd & Mitchell (1984), so that the induced magnetic field is negligible, while the applied field can be considered as constant. The interaction parameter N and the square of the Hartmann number M represent the relative importance of the electromagnetic body forces and the inertial and the viscous ones, respectively. The typical values of M and N in lithium or lithium–lead cooled fusion reactors are 10^3–10^4 for M and 10^2–10^5 for N. The wall conductance ratio c, which expresses the ratio of wall conductance to that of the fluid, is of the order of 10^{-2}–10^{-1}.

Consider the flow in a right-angle bend as shown in figure 1. This bend consists of a duct parallel to the magnetic field, which will be called the toroidal duct, and a duct perpendicular to the field, which will be called the radial duct (according to the blanket concept presented by Malang *et al.* 1988). The inclination Θ of the magnetic field to the toroidal-duct walls does not exceed 15°, which is the maximum field inclination with respect to the toroidal ducts in a fusion blanket.

Before outlining some results for MHD bend flows which have been obtained in the past by several authors, some phenomenological aspects should be discussed. Consider first the flow for $\Theta = 0°$. If both radial and toroidal ducts are long enough, fully developed velocity profiles are established at a certain distance from the junction. In the toroidal duct this distance is $O(M)$ for $N \gg M^{3/2}$, see Molokov & Bühler (1994), while the velocity profile is of Poiseuille type. In the radial duct the distance is $O(1)$, while the profile is M-shaped (Hunt 1965; Walker 1981). In the core of the radial duct the velocity is constant, while part of the volume flux is carried by high-velocity jets in so-called parallel layers. They are formed near the walls, parallel to the magnetic field.

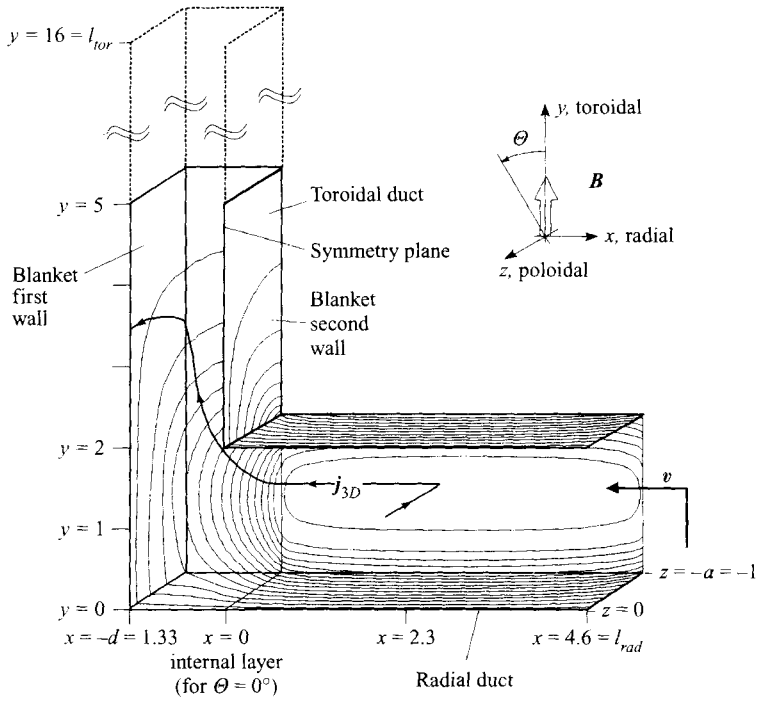

FIGURE 1. Schematics and coordinate system of one half of the bend flow ($z < 0$) studied. Also shown are the isolines of the induced wall potentials for the experimental geometry for an inclination angle of $\Theta = 0°$, $c = 0.052$ calculated with the asymptotic model presented in §3. The distance between the isolines is $\Delta\Phi = 0.05$.

The thickness of the parallel layers is determined by viscous–electromagnetic interaction and is $O(M^{-1/2})$. The velocity in these layers is $O(M^{1/2})$.

Consider now the events at the junction $x = 0$. Owing to Ohm's law for a moving conducting fluid an electric potential is induced in the radial duct where the flow is essentially perpendicular to the magnetic field, whereas no potential is induced very far from the junction in the toroidal duct where the flow and the magnetic field are parallel. The potential difference occurring in the flow direction drives the so-called three-dimensional electric current $\boldsymbol{j}_{3D}$, which may short-circuit in the way qualitatively shown in figure 1. The x-component of this current results in a Lorentz-force $\boldsymbol{j}_{3D,x} \times \boldsymbol{B}$, which leads to a thrust of the fluid towards the sidewalls thus enhancing the M-shape of the velocity profile. At the junction $x = 0$ a parallel, internal layer is formed, which separates cores of radial and toroidal ducts.

For $\Theta = 0°$ an asymptotic inertialess theory has been developed by Molokov & Bühler (1994) for a U-bend and for a right-angle bend under the assumptions $N \gg M^{3/2} \gg 1$ and $c \gg M^{-1/2}$. The latter assumption means that the currents conducted by the parallel layers are negligible with respect to wall currents. The theory predicts that the $O(1)$ y-component of the core velocity in the toroidal duct vanishes, so that all the fluid is carried in the y-direction in the parallel layers. The parallel layers in the toroidal duct merge at distances $O(M)$ from the junction, so that in practice the fully developed Poiseuille velocity profile in this duct will never be established. In addition, the theory predicts no $O(1)$ pressure drop in the toroidal duct.

The main assumption of the asymptotic theory is that the flow is inertialess. In three-dimensional MHD flows inertia effects play a significant role due to local accelerations

and braking of the fluid. One can expect that, in particular, the parallel layers with the high-velocity jets are more affected by inertial effects than the core flow. Inertial forces in the parallel layers become important for $N = O(M^{3/2})$ and dominant for $N \ll M^{3/2}$. In the latter case the thickness of these layers becomes $O(N^{-1/3})$, and the flow in the layers is determined by electromagnetic–inertia interaction. Effectively, the inertial contribution to the pressure drop is of the order of $N^{-1/3}$ (see § 5.1.2). These asymptotic estimates have been suggested by Hunt & Holroyd (1977), who based their analysis on the work of Hunt & Leibovich (1967). For $N = O(M^{3/2})$ and for $N \ll M^{3/2}$ no adequate theoretical results exist for bend flows or for general three-dimensional MHD duct flows except these simple asymptotic estimates (see the discussion by Molokov, Bühler & Stieglitz 1994). Thus experimental studies of bend flows are of particular importance. Most of these studies have been performed for bends of circular cross-section, which are significantly different from rectangular ones. Therefore, these studies are not directly related to the present one. An appropriate review of these flows can be found in Hunt & Holroyd (1977) and Holroyd & Hunt (1980). What is similar in flows in circular and rectangular bends is the formation of the internal layer, which has the same asymptotic thickness in both cases. Therefore, the inertial contribution to the pressure drop should vary similarly with N.

At attempt to prove the $N^{-1/3}$-dependence experimentally has been made by Holroyd (1979) in a radial–toroidal–radial Z-shaped bend of circular cross-section with the wall conductance ratio of $c = 0.155$ at relatively low $M \approx 230$ and low $N \approx 10^1$–10^2. Although the experimental data for pressure suggest $N^{-1/3}$-dependence, the accuracy of the measurements did not allow final proof of this important relation. The results of most of the other authors were contradictory and led to a great degree of confusion. The pressure drop due to inertial effects varied from N^{-1} (180° bend of circular cross-section, Bocheninskii, Tananaev & Yakovlev 1977), which corresponds to very fast decay of the inertia effects with N, to $N^{-0.1}$ (U-bend of circular cross-section, Grinberg, Kaudze & Lielausis 1985), which corresponds presumably to negligible inertia effects. The exponent $-1/3$ has never appeared (see the critical reviews by Holroyd 1979, 1980 and Molokov *et al.* 1994). The first series of experiments carried out by Barleon *et al.* (1992, 1993*a*, *b*) in a right-angle bend of rectangular cross-section clarified that inertia effects play a significant role in radial–toroidal bends, which suggests that a more detailed analysis of the phenomenon is necessary.

It is very important to note that the type of variation of the pressure drop with N and M is of fundamental importance not only for bend flows but for general three-dimensional MHD flows. The reason is that the exponents of N and M characterize the type of flow pattern that is established and the main effects that determine this pattern. Thus, the experimental results suggest how the actual theoretical models require improvement. In particular, the $N^{-1/3}$-dependence indicates that the core may be considered as inviscid and inertialess, while the parallel layers are governed by electromagnetic–inertia interaction.

This paper presents a comprehensive experimental study of the flow in a right-angle bend with the following main objectives:

(i) to determine the range of validity of the asymptotic flow model developed for $N \gg M^{3/2}$.

(ii) to verify Hunt & Holroyd's estimates of $N^{-1/3}$ of the thickness of parallel layers for $N \gg M^{3/2}$,

(iii) to determine the scaling laws for the pressure drop in the wide range of parameter variation for $N \gg M^{3/2}$ as well as for $N \ll M^{3/2}$, for which no theoretical results exist.

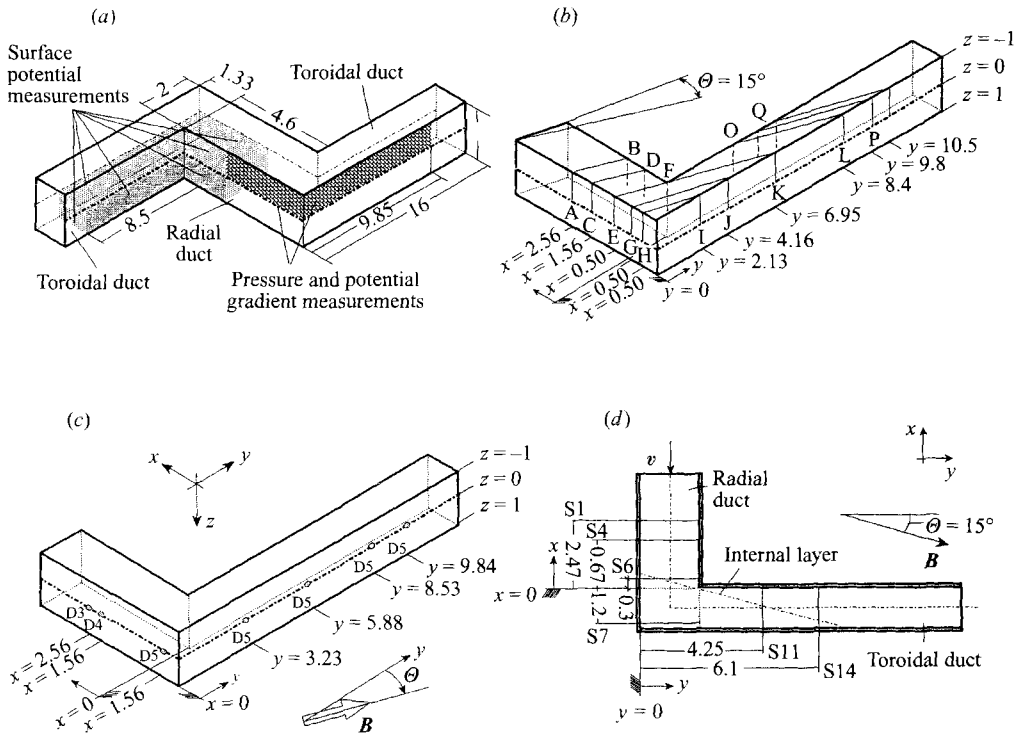

FIGURE 2. (*a*) Geometrical dimensions of the Z-shaped test section. (*b*) Location of the wall potential measurement lines. (*c*) Location of the pressure taps in the test section. (*d*) Location of the traversable potential probes.

A comparison of the experimental data and theoretical results is performed mainly for pressure and wall potentials. These quantities can be measured very precisely. Measurements of the potential gradient within the liquid metal are less accurate and difficult to interpret (cf. §5.2.2 and the Appendix).

In §5.1 the results for $\Theta = 0°$ are presented, while the effects of field inclinations are studied in §5.2. In both cases numerical results are discussed first, and then compared with the experiment.

2. Formulation

The MHD bend flow under consideration is studied in a Z-shaped geometry as shown in figure 2(*a*), which has been chosen in order to fit best the experimental facility. The dimensionless equations governing the MHD flow in the inductionless limit as $R_m \to 0$ are the conservation of:

momentum
$$\frac{1}{N}\left[\frac{\partial \boldsymbol{v}}{\partial t} + (\boldsymbol{v}\cdot\nabla)\,\boldsymbol{v}\right] = -\nabla p + \frac{1}{M^2}\Delta \boldsymbol{v} + \boldsymbol{j}\times\boldsymbol{B}, \tag{2.1}$$

mass
$$\nabla\cdot\boldsymbol{v} = 0, \tag{2.2}$$

charge
$$\nabla\cdot\boldsymbol{j} = 0; \tag{2.3}$$

and Ohm's law
$$\boldsymbol{j} = -\nabla\Phi + \boldsymbol{v}\times\boldsymbol{B}. \tag{2.4}$$

Here, $\boldsymbol{v} = (u, v, w)$, $\boldsymbol{B} = (-\sin\Theta, \cos\Theta, 0)$, j, ϕ,p and t denote the dimensionless velocity, the magnetic induction, the electric current density, the electric potential, the pressure and time, scaled with the characteristic values v_0, B_0, $\sigma v_0 B_0$, $a v_0 B_0$, $a\sigma v_0 B_0^2$, and a/v_0, respectively. In the theoretical consideration the magnetic field is assumed to be uniform.

The boundary conditions at the duct walls are the no-slip condition

$$\boldsymbol{v}|_{Wall} = 0, \tag{2.5}$$

and the thin-wall condition (see Walker 1981)

$$\boldsymbol{j}\cdot\boldsymbol{n} = c\nabla_\perp^2 \Phi_W, \tag{2.6}$$

where $\boldsymbol{n}$ is the inward unit normal to the wall, and $\nabla_\perp$ denotes the projection of the gradient on the wall surface. The thin-wall condition describes the balance of charge in the conducting duct walls. The currents $(-\boldsymbol{j}\cdot\boldsymbol{n})$ from the fluid to the wall enter this balance as a source term. If the fluid is in perfect electrical contact with the duct walls so that there is no contact resistance across the fluid–wall interface, the potential of the wall and that of the adjacent fluid are equal, i.e. $\Phi_W = \Phi$ at the interface.

If the toroidal ducts are long enough, fully developed conditions are established with

$$\frac{\partial p}{\partial y} = \text{const.}, \quad \frac{\partial \Phi}{\partial y} = u = w = 0 \quad \text{as} \quad y \to \pm\infty. \tag{2.7}$$

If $\Theta = 0°$, the conditions $\partial p/\partial y = \text{const.}$, $\partial\Phi/\partial y = 0$ still hold but the conditions $p = \text{constant}$, $\Phi = 0$ seem more appropriate because no currents are induced in field-aligned flows.

3. Analysis

The steady, inertialess versions of equations (2.1)–(2.7) are analysed by asymptotic methods for $N \gg M^{3/2} \gg 1$ and for $c \gg M^{-1/2}$ (see Moon & Walker 1990; Moon *et al.* 1991; Hua & Walker 1991; Bühler 1993, 1995, and Molokov & Bühler, 1994, 1995).

For $\Theta = 0°$ the analysis follows the line taken by Molokov & Bühler (1994). The only modification is in the boundary conditions in the radial duct, which is discussed below.

The flow in one 90° bend becomes independent of the flow in the other one if the radial-duct length l_{rad} (see figure 1) is sufficiently large, i.e. if fully developed MHD flow is established at $x = 1/2 l_{rad}$. This allows the computational effort to be reduced by considering only the part with $x < 1/2\ l_{rad}$ and assuming fully developed flow conditions

$$\frac{\partial p}{\partial x} = \text{const.}; \quad \frac{\partial \Phi}{\partial x} = v = w = 0 \quad \text{at} \quad x = 1/2\, l_{rad}. \tag{3.1}$$

These flow conditions were assumed in Molokov & Bühler's calculations. For calculations where these conditions are not satisfied (in the present case $1/2\, l_{rad}$ is only 2.3) the computational domain is extended to $x = l_{rad}$ with appropriate symmetry conditions between $x = 0$ and $x = l_{rad}$ applied at $x = l_{rad}$. This is justified in inertialess flows. For potentials this symmetry condition reads

$$\Phi(l_{rad}, y, z) = \Phi(0, 2a - y, z). \tag{3.2}$$

This change in the boundary condition does not lead to qualitatively new results, but for $x = 1/2l_{rad} = 2.3$ the flow in the radial duct turns out to be slightly different from fully developed.

Flows with $\Theta = 0°$ are calculated by the use of the numerical code developed by Bühler (1995). This code has been designed for calculations of three-dimensional inertialess MHD flows in ducts of arbitrary geometry.

In both cases $\Theta = 0°$ and $\Theta \neq 0°$ the same asumptions are made and both methods take advantage of specific properties of MHD flows in strong fields. The most essential one is the fact that the pressure does not vary along magnetic field lines as $M, N \to \infty$ (Kulikovskii 1968). This can be easily seen by multiplying equation (2.1) by $\boldsymbol{B}$, which reduces to

$$\boldsymbol{B}\cdot\nabla p = 0 \quad \text{as} \quad M, N \to \infty. \tag{3.3}$$

This allows an analytical integration of the basic equations in magnetic field direction. The integration functions can be related to the wall potential Φ_W and to the pressure p, the leading variables in the analysis. Once Φ_W and p are determined, the whole three-dimensional flow can be reconstructed. While the approach proposed by Molokov & Bühler (1994) uses an iterative method to determine pressure and wall potential in rectangular subdomains, the code proposed by Bühler (1995) uses a direct linear solver to determine the solution on a boundary-fitted grid.

4. Experimental set-up

The experiments in the Z-shaped test section have been performed in the MEKKA facility (Magneto-Hydrodynamik-Experiment in Natrium-Kalium Karlsruhe) of the Forschungszentrum Karlsruhe. Here only a brief overview of the experimental facility is given, a more detailed description may be taken from Barleon, Casal & Lenhart (1991).

The magnet used in the experiment is a liquid-helium-cooled super-conducting solenoid magnet with a maximum magnetic field strength of 3.6 Tesla. The cylindrical space has a diameter of 400 mm. The position of the test section in the magnet was chosen in such a way as to provide an almost homogeneous field over the whole of the radial–toroidal bend. The variations of the magnetic field strength over the part of the test section of interest shows deviations of less than 10% in a length of 450 mm. The mapping of the absolute magnetic induction of the cylinder-symmetrical field is shown as isolines in figure 3, together with the magnetic field vectors.

A centrifugal pump with a maximum pressure head of 0.9 MPa at a flow rate of 22 $m^3\,h^{-1}$ circulates the eutectic sodium-potassium alloy $Na^{22}K^{78}$ (melting point -11 °C) at temperatures below 250 °C. The thermophysical properties of the alloy have been described in detail by O'Donnell, Papanicolaou & Reed (1989). An additional electromagnetic pump is used for high-temperature wetting procedures above 250 °C and also for very low flow rates. During the wetting procedure impurities on the steel surface, such as oxygen or alloy components are dissolved in the NaK. With this procedure a perfect electrical contact between the structural material and the fluid without contact resistance is ensured. The dissipated energy in the loop is removed by an oil-cooled double-tube heat exchanger.

The flow rate is measured simultaneously by a gyrostatic mass flow meter and by an electromagnetic flow meter in order to have two different measurement principles to determine the flow rate. Both agreed throughout the measurements with an accuracy of 0.5%.

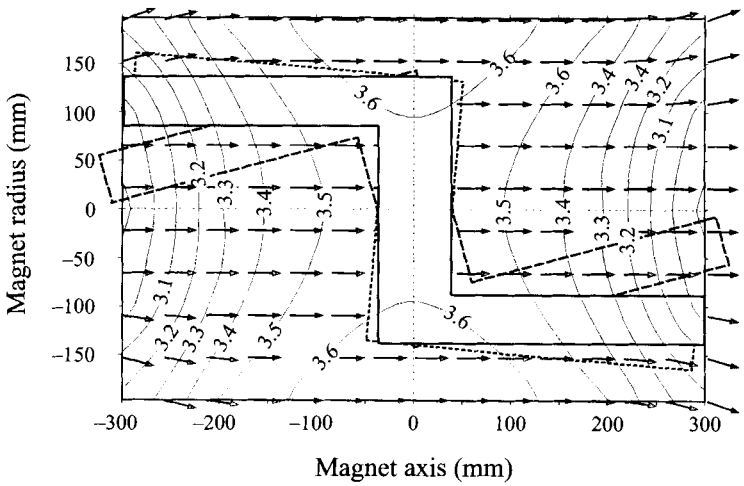

FIGURE 3. The isoline graph shows the total magnetic induction $|B|$ of the magnet used in the experiment. The overlayed vector plot shows the magnetic field vector orientation in the magnet. The Z-shaped test section is shown as a straight line. The other inclination angles investigated, $\Theta = -5°$ (-------) and $\Theta = 15°$ (---) are also indicated.

The entire loop can be moved on rails together with the test section along the axis of the magnet. A valve station interconnected in the inlet and outlet lines of the test section allows a reversal of the flow direction within the test module.

The test section itself was designed in joint work of the Forschungszentrum Karlsruhe with the Argonne National Laboratory (ANL) and was fabricated at the ANL. The rectangular ducts are made of 4.45 mm thick stainless steel plates welded together by electron beam welding to ensure sharp corners. The section is designed as a symmetric Z-bend. Half the distance between the Hartmann walls in the radial duct is $a = 38.1$ mm. This gives a wall conductance ratio of $c = 0.052$. All other length scales of the test section, which are normalized with a may be taken from figure 2(a). The measurement of the wall potentials was performed in one half of the test section, whereas the pressure measurements were carried out in the other half.

In order to measure the electric wall potentials 141 spring-loaded needles, mounted on fibreglass plates, are attached to the test section. The needles are in electric contact with the steel walls of the duct. They are arranged in 9 lines with 13–17 probes in each line at an angle of $\Theta = 15°$ with respect to the toroidal duct branch, see figure 2(b). The electric potential at a defined location is measured as a potential difference with respect to a fixed reference potential originating from one needle welded on the duct wall in the plane $z = 0$.

The pressure measurements have been carried out using stainless steel tubes welded on the duct wall centreline. Four unipolar capacitive pressure transducers of different measurement ranges (0–10, 0–370, 0–1860, 0–4000 mbar) are arranged in parallel to measure the pressure differences between two locations. The maximal resolution of the pressure transducers is ± 0.3 mbars. The exact location of the pressure holes is shown in figure 2(c).

When measuring pressures in three-dimensional MHD flows a phenomenon appears which is not known in conventional hydrodynamics. Directly measured pressure differences do not represent the real pressure differences between two locations in the duct. A virtual pressure is superimposed on the real pressure in the duct. For example, in the toroidal duct at $x = -1.33$ the component of current j_z flows normal to the

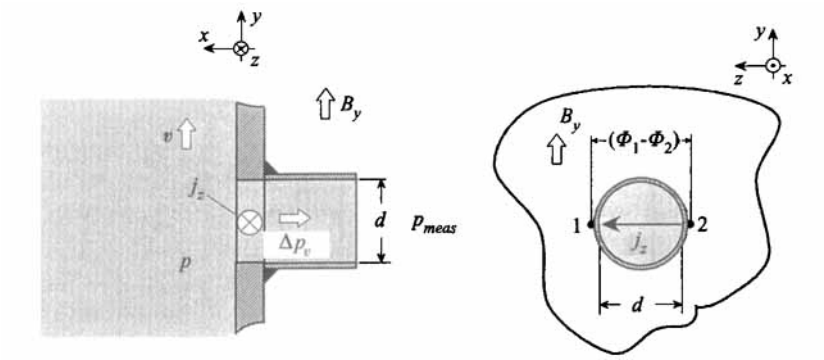

FIGURE 4. Physical mechanism showing the appearance of an additional virtual pressure superposed on the real pressure.

magnetic field component B_y, see figure 4. This virtual pressure may reach significant values. For example, for an inclination angle of $\Theta = 15°$ the maximum virtual pressure correction in $\Delta p_v = 0.012$ (a dimensional value of 148 mbar!) at the position D8.

But, by measuring the potential difference $\Phi_2 - \Phi_1$ with the potential probes directly at the stainless steel tube (figure 4) this virtual pressure can be estimated. Using simple considerations an analytical correlation for the pressure correction at the measuring hole can be deduced. The force balance at the pressure tap reads

$$\boldsymbol{n}\cdot\nabla p = \boldsymbol{n}\cdot(\boldsymbol{j}\times\boldsymbol{B}). \tag{4.1}$$

Ohm's law formulates the relation between the current density and the wall potentials, assuming stagnant fluid in the tap ($\boldsymbol{v} = 0$):

$$\boldsymbol{n}\cdot\nabla p = -\boldsymbol{n}\cdot(\nabla\Phi_W\times\boldsymbol{B}). \tag{4.2}$$

Integrating (4.2) over the thickness of the duct wall one obtains for the dimensionless virtual pressure jump Δp_v at the pressure tap:

$$\Delta p_v = -\frac{t_W}{d}(\Phi_2 - \Phi_1). \tag{4.3}$$

Herein, d denotes the gap of the pressure tap, which is $d = 3.2$ mm in the experiment, and t_W the wall thickness. $(\Phi_2 - \Phi_1)$ is the measured potential difference in the z-direction at the steel tube, see figure 4.

In this experiment local potential gradient measurements within the fluid have also been made with LEVI probes. The measuring principle of these LEVI-probes is described in the Appendix (see also Reed & Picologlou 1986), where their applicability to three-dimensional MHD-flows is also considered. The exact locations of the traverses of the sensing tips indicated as S1, S4, S6, S7, S11 and S14 may be taken from figure 2(*d*). Since the probe measurements may significantly influence the MHD bend flow these measurements were carried out independently from the wall potential and the pressure measurements.

The experimentally obtained dimensionless data plotted in the figures that follow are values which have an absolute error of less than 5% using the Gaussian error propagation law. If this error margin is exceeded, it is indicated by error bars. This holds in particular for the pressure measurements, where extremely low pressures at low flow rates are obtained and thus the resulting absolute error is higher than in the potential measurements.

5. Results and discussion

5.1. $\Phi = 0°$

5.1.1. *Numerical results*

The calculated isolines of the wall electric potential for the experimental geometry are shown in figure 1. The wall current is perpendicular to the isolines. The main flow characteristics have been outlined in the Introduction and are generally the same as those described by Molokov & Bühler (1994). As the flow approaches the junction, the fluid is pushed towards the sidewalls, and the sidewall jets increase in magnitude. The fluid in the toroidal duct is transported in the y-direction in the parallel layers, since the y-component of the core velocity vanishes. The flow distribution among the layers is shown in figure 5. A recirculating flow in the toroidal duct is predicted, which is associated with the negative flow rate Q_2 in the major part of the toroidal duct.

The question of the pressure drop is very important. In the radial duct the pressure drop between any two points along the flow may be split into two parts. The first part, the so-called two-dimensional pressure drop Δp_{2D} may be estimated using the approximate expression for the fully developed pressure gradient

$$\left(\frac{\mathrm{d}p}{\mathrm{d}x}\right)_{2D} = -\left[\frac{1}{3}\frac{M^{1/2}}{1+cM^{1/2}} + \frac{1+c}{c+1/M}\right]^{-1}, \tag{5.1}$$

see Tillack (1990). A more precise but also a more complicated expression for $c \gg M^{-1}$ has been derived by Molokov (1993). The second part, the so-called three-dimensional pressure drop Δp_{3D}, which expresses the excess pressure drop required for reshaping the velocity profile near the junction, can be written in the form

$$\Delta p_{3D} = \Delta p_{3D,C}(M, N \to \infty) + \Delta p_{3D,N}(N) + \Delta p_{3D,M}(M). \tag{5.2}$$

Even in inviscid and inertialess flows, in which only Lorentz and pressure forces appear, a three-dimensional pressure drop $\Delta p_{3D,C}$ caused by Joulean dissipation of three-dimensional electric currents is present. The second and third terms in equation (5.2) represent the contribution of parallel layers with electromagnetic–inertia and viscous–electromagnetic interaction, respectively. The first term may be calculated with the asymptotic flow model presented here. Both other contributions could up to now be determined only experimentally. The formula (5.2) neglects the interaction of viscous–inertia effects, which are present in a real MHD flow if both effects on pressure drop are comparable.

In the toroidal duct both Δp_{2D} and $\Delta p_{3D,C}$ vanish.

The total pressure drop may also be represented in the form

$$\Delta p = \Delta p_C(M, N \to \infty) + \Delta p_{3D,N}(N) + \Delta p_{3D,M}(M). \tag{5.3}$$

In this case the first and the third terms on the right-hand side contain contributions from the two-dimensional pressure drop.

Figure 6 shows the calculated pressure distribution along the radial duct for the investigated test section in different planes z = constant. Near the two toroidal ducts at $x = 0$ and $x = 4.6$ the strongest deviations between the three- and the two-dimensional flow appear. With increasing distance from the toroidal ducts towards the symmetry plane $x = 2.3$ the three-dimensional effects on the pressure decrease, but even at $x = 2.3$ they are still present. The pressure gradient there is approximately 4.5% higher than that of a two-dimensional MHD flow. Owing to inertia effects the deviations from the fully developed conditions are expected to be even higher, so that

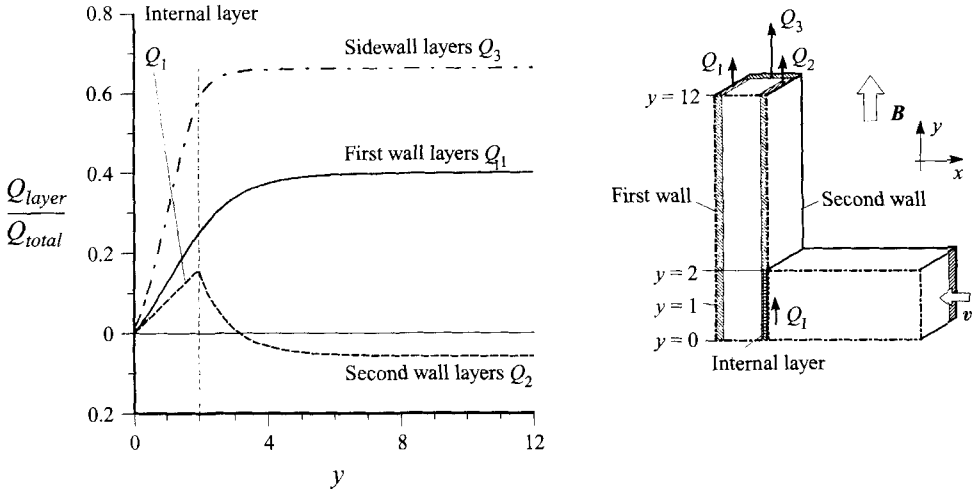

FIGURE 5. Calculated volumetric flow rates carried by different boundary layers related to the total flow rate in the toroidal duct for $c = 0.052$; $\Theta = 0°$.

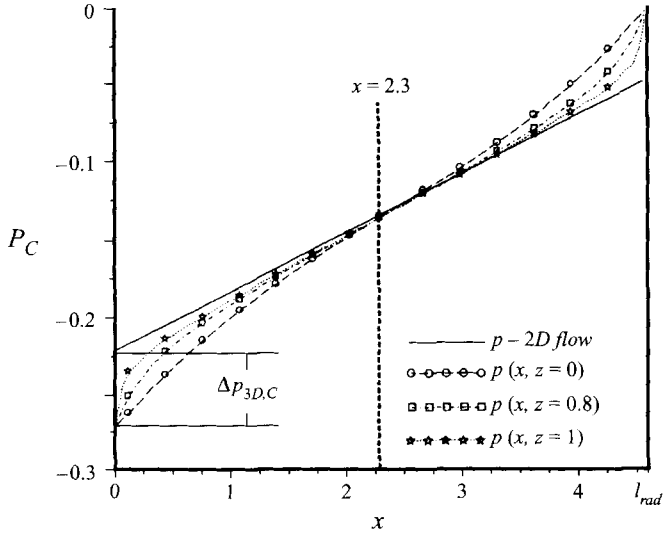

FIGURE 6. Calculated axial pressure distribution in the radial duct for different z-coordinates compared with the fully developed two-dimensional flow for $c = 0.052$; $\Theta = 0°$.

in reality the flow will never be fully developed in the entire test section. The calculated three-dimensional pressure drop between $x = 0$ and $x = 2.3$ is $\Delta p_{3D,C} = 0.05$.

The numerically obtained data will be compared in the next subsection with the experimentally measured values.

5.1.2. *Experimental results for* $\Theta = 0°$

(*a*) *Potential measurements*

In the presentation of the experimental results only characteristic values at selected positions are shown. Other results not presented here show the same tendency.

First, the symmetry of the flow with respect to the plane $z = 0$ has been investigated in order to confirm the geometrical arrangement of the test section with respect to the orientation of the magnetic field. Figure 7 shows the potential measurements at

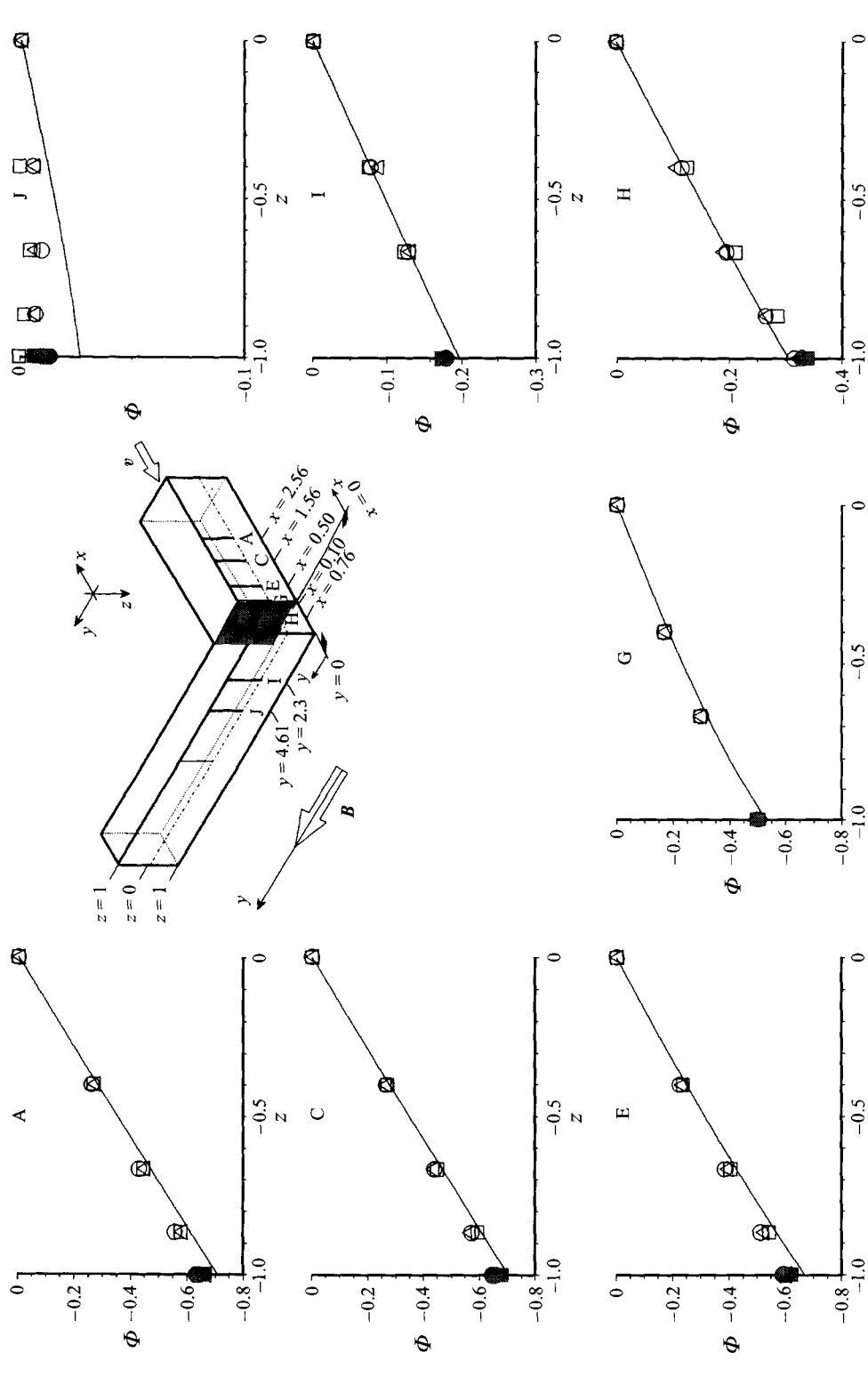

FIGURE 7. Wall potentials at lines A, C, E, G, H, I, and J for different M; $N = 1290$; $c = 0.052$, $\Theta = 0°$; radial → toroidal flow. ○, $M = 8177$; □, $M = 4081$; △, $M = 1990$; ——, calculated potential distribution (M, $N \to \infty$). The filled symbols drawn at the positions $z = -1$ indicate the negative potential $-\Phi(z = 1)$ measured at the position $z = 1$ in order to check the symmetry condition.

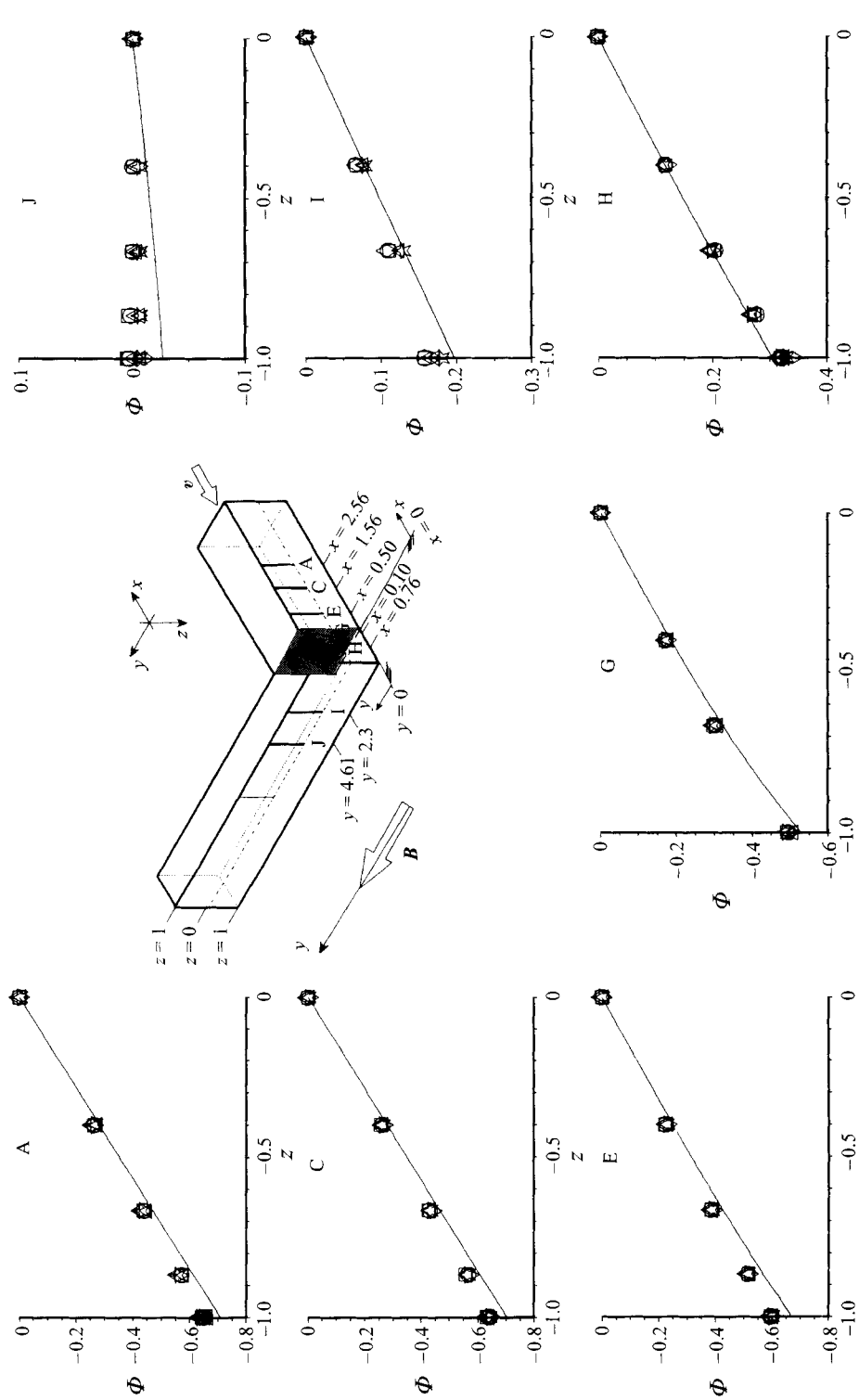

FIGURE 8. Wall potentials at lines A, C, E, G, H, I and J for different N; $M = 8177$; $c = 0.052$, $\Theta = 0°$; radial→toroidal flow. ○, $N = 26390$; □, $N = 19321$; △, $N = 5721$; ◇, $N = 3556$; ☆, $N = 1851$; ——, calculated potential distribution (M, $N \to \infty$).

positions A, C, E, G, H, I and J for $-1 \leqslant z \leqslant 0$ for different Hartmann numbers at a constant value of $N = 1920$. To check the symmetry the negative values of the potential at $z = \pm 1$ (filled symbols) and included in figure 7. The differences in all positions between $-\Phi(z = 1)$ and $\Phi(z = -1)$ are within the accuracy of measurement, so that the flow is symmetric with respect to the plane $z = 0$. No significant influence of the Hartmann number on the potential of the first wall (see figure 1) of the toroidal duct nor on the Hartmann walls of the radial duct can be observed within the investigated range of M. The agreement between the measured and the calculated values is very good.

Potential measurements at the same positions for a constant Hartmann number at different values of the interaction parameter in the range $N = 1.8 \times 10^3$–2.6×10^4 exhibit similar behaviour with no significant influence of N at the same positions, see figure 8. The agreement with the numerically calculated data is good, even for the corner regions. The deviations that appear between the model and the measurement are below 10%.

The potential on the Hartmann walls Φ_{WH} is equal to the core potential Φ_C at the same position for large M; $(\Phi_{WH} - \Phi_C)$ is of $O(M^{-2})$ according to Walker, Ludford & Hunt (1972). Thus, the potential measurements on the Hartmann walls reveal that even at the lowest values of $M \approx 2 \times 10^3$ and $N \approx 2 \times 10^3$ the flow in the core is inertialess and inviscid.

Figure 9 shows the potential distributions on a toroidal sidewall for different values of N at positions $x =$ constant as a function of y. In the vicinity of the bend in the sidewalls in the region $-1.33 \leqslant x \leqslant -0.1$ and $0 \leqslant y \leqslant 3$ a dependence of the sidewall potential on the interaction parameter is found, in contrast to the Hartmann walls, where such a dependence could not be detected. For high N the experimental values tend to the asymptotic ones. However, even for the highest values of N investigated, the magnitude of the measured wall potentials in this region is higher than the calculated values.

In contrast, in the radial duct no significant influence of inertia on the sidewall potential was observed for the same parameters, except for the immediate vicinity of the inner corner at $y = 2$. The sidewall potentials at a characteristic position in the radial duct near the inner corner ($x = 0.22$; $y = 1.87$) are plotted in figure 10 versus an axis scaled with $N^{-1/3}$ to demonstrate clearly the linear dependence of the inertial part of the potential on this quantity. Figure 10 shows in addition the calculated asymptotic value. For high values of N, i.e. as $N^{-1/3} \to 0$ the measured values tend asymptotically towards the theoretical result. The same dependence on N has been observed at the sidewalls of the toroidal duct. Figure 10 further reveals that inertia effects would become small when N exceeds a value larger than about $M^{3/2}$ in accordance with predictions by Hunt & Holroyd (1977). The measured dependence of the sidewall potential on $N^{-1/3}$ agrees with the scaling law for the thickness of inertial side layers suggested by Hunt & Holroyd (1977). It has never been shown experimentally up to now with such an accuracy.

The absolute value of the measured sidewall potential in the radial duct near the bend in a radial → toroidal flow is higher than in a toroidal → radial flow, see figure 10. An explanation for this could be that, in the radial → toroidal case, directly beyond the corner at $x < 0$, $y > 2$ a separation zone may develop along the second wall. Because of the previously discussed conditions this zone is pressed towards the second wall. It persists over long toroidal distances and remains rather thin so that its Ohmic resistance is relatively high. For the reversed flow direction the separation area may develop near the top Hartmann wall at $x > 0$, $y < 2$. Compared to the previously

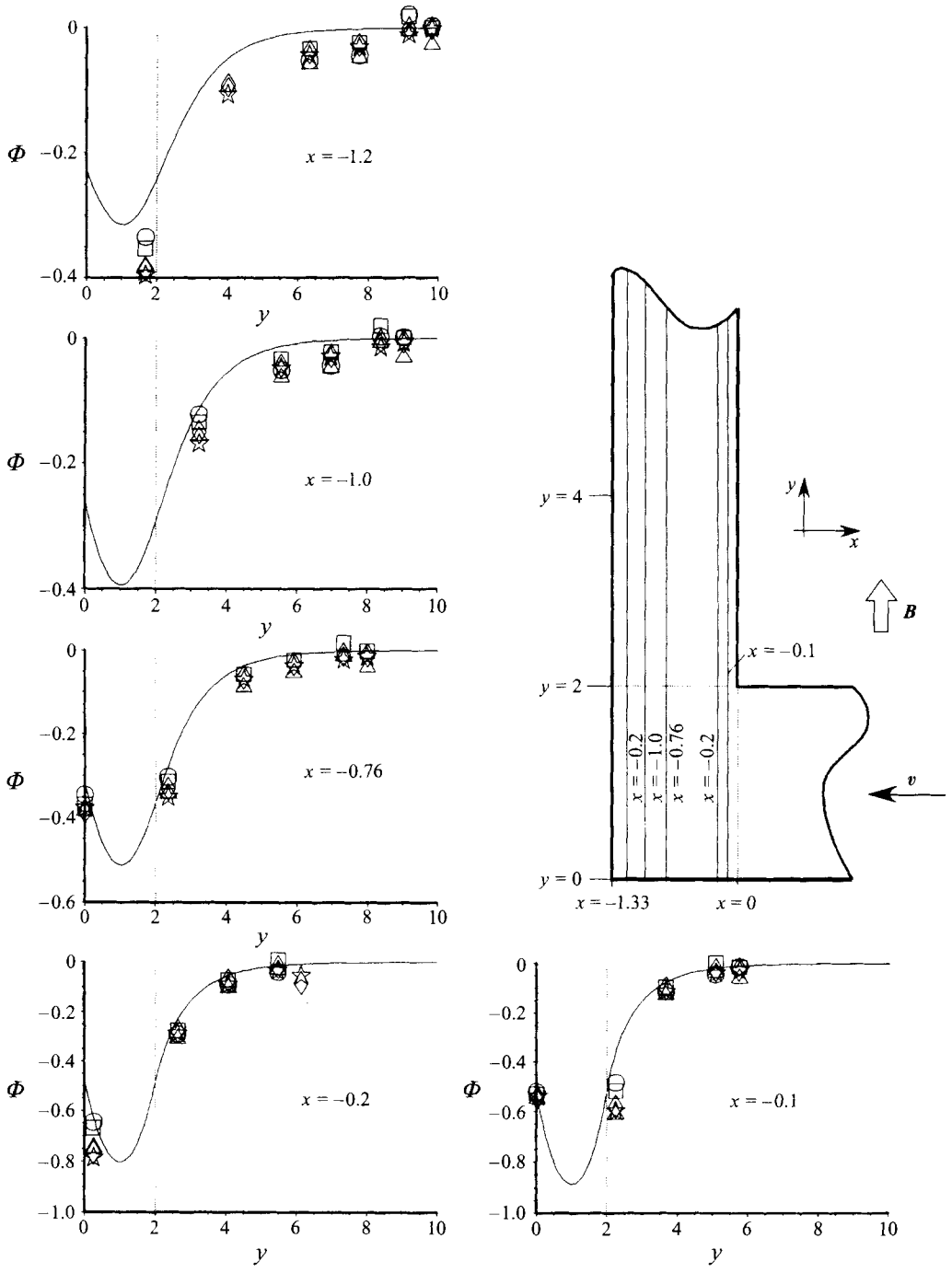

FIGURE 9. Wall potentials on the sidewall of the toroidal duct at lines x = constant, $M = 8177$; $c = 0.052$; $\Theta = 0°$; radial → toroidal flow. ○, $N = 26390$; □, $N = 19321$; △, $N = 5721$; ◇, $N = 3556$; ☆, $N = 1851$; ——, calculated potential distribution (M, $N \to \infty$).

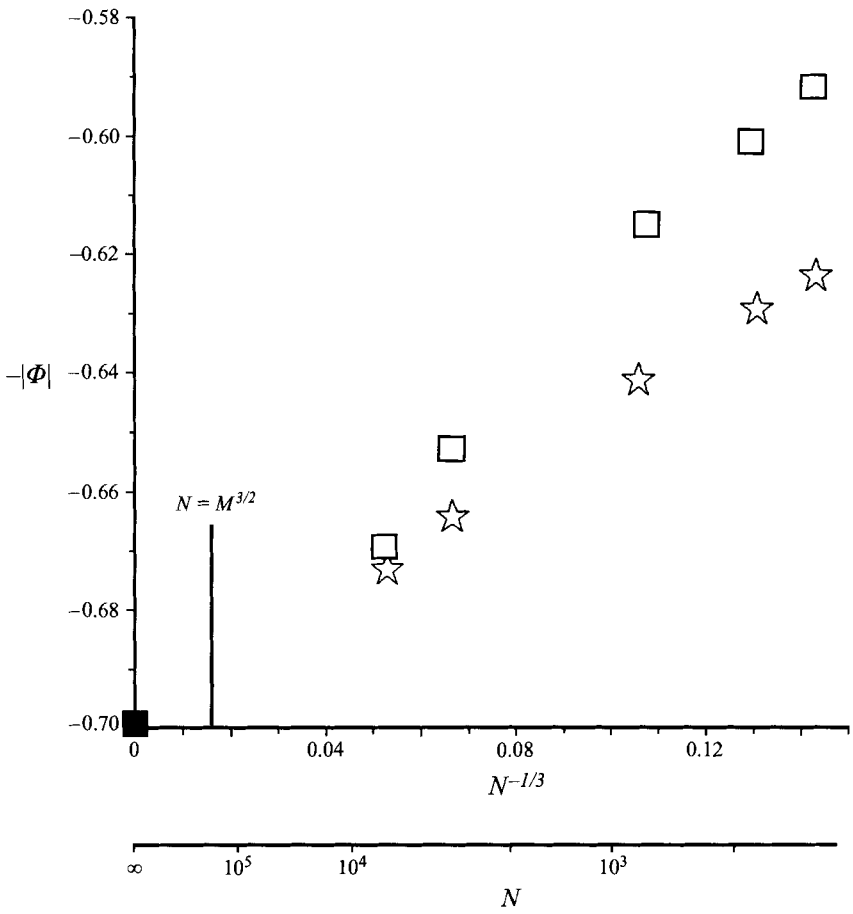

FIGURE 10. Measured side wall potential at the point $x = 0.22$; $y = 1.87$; $M = 3978$ as a function of $N^{-1/3}$, $\Theta = 0°$, $c = 0.052$; ☆, radial–toroidal flow; □, toroidal–radial flow. The filled symbol represents the value calculated for M, $N \to \infty$.

discussed case it will be much shorter but it can be thicker. The induced potential in this separation area is lower. Therefore, the Ohmic resistance of the zone in the toroidal → radial flow is smaller, which leads to a higher current and thus to a higher pressure drop, as will be shown below.

(*b*) *Pressure measurements*

All pressure measurements discussed were performed on the symmetry plane $z = 0$. The results shown in figures 11–14 represent the pressure at the fluid–wall interface, obtained by correction of the real measured pressure with the pressure difference induced by wall currents across the duct wall bore according to equation (4.3).

In the asymptotic model the pressure is constant along magnetic field lines according to equation (3.3). A good agreement between the theoretical results and the measured values has been found at high N. The deviations from the asymptotic theory at high N are small compared to the total pressure drop between D3 and D9, which is about 0.14.

In figure 11(*a*, *b*) the pressure differences between D5 and D6, and D6 and D7 are shown as a function of N. Deviations between model and measurement for high N are

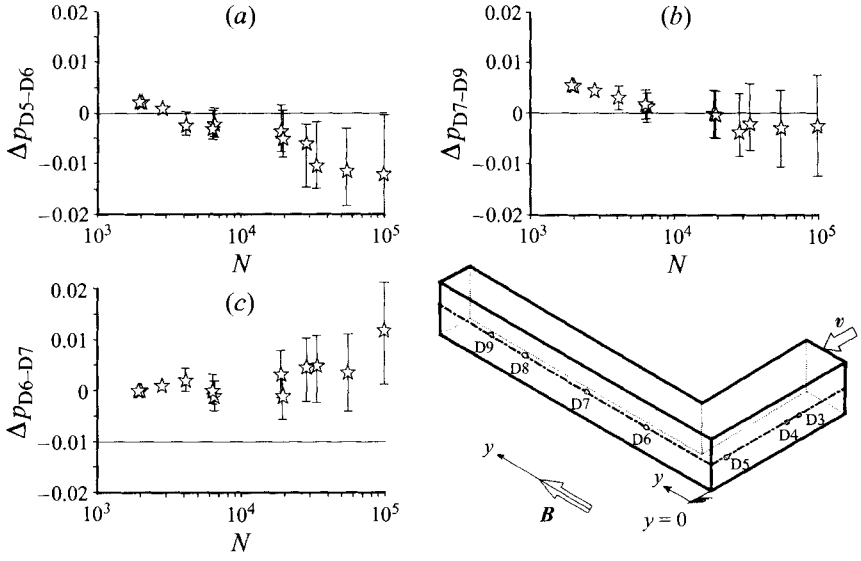

FIGURE 11. Pressure differences in the toroidal duct between (*a*) D5 and D6, (*b*) D6 and D7, and (*c*) D7 and D9 for $M = 7851$; $c = 0.052$; $\Theta = 0°$ and radial → toroidal flow. ——, Pressure drop predicted by the asymptotic model as $M, N \to \infty$.

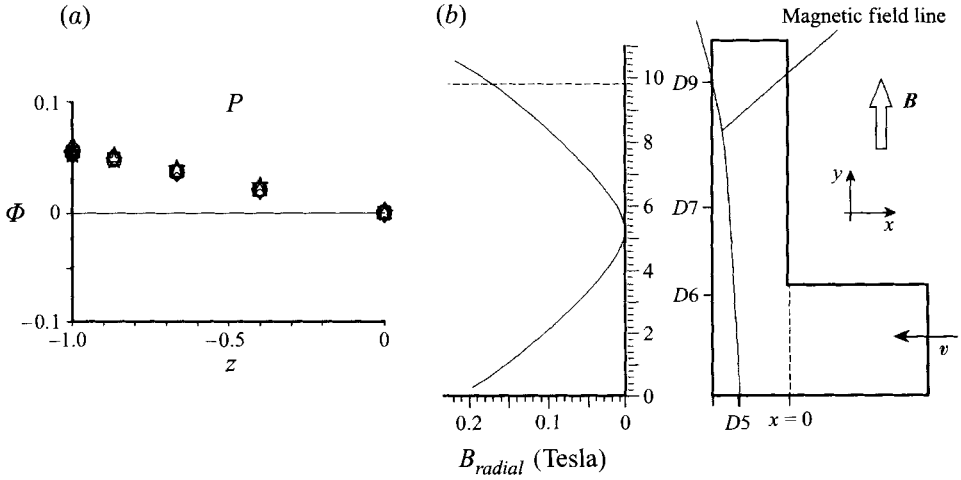

FIGURE 12. Influence of the radial magnetic field component on the measured potential and pressure distribution. (*a*) Measured wall potential at the line P for $M = 8177$; $c = 0.052$; $\Theta = 0°$ and radial → toroidal flow. ○, $N = 26390$; □, $N = 19321$; △, $N = 5721$; ◇, $N = 3556$; ☆, $N = 1851$; ——, calculated potential distribution ($M, N \to \infty$). (*b*) Radial magnetic field strength in Tesla in the plane $x = -1.33$ as a function of y.

caused by the resolution of the pressure transducers at extremely low pressures for small flow rates. The measured differences to the model prediction occurring between D7 and D9, see figure 11(*c*), are not caused by measurement errors. They arise from the weak inhomogeneity of the magnetic field. This can be confirmed by the potential measurements at station P shown in figure 12(*a*). The potential there is positive, while in the rest of the duct for $z < 0$ it is negative. The absolute strength of the radial component of the magnetic field at $x = -1.33$ along y is shown in figure 12(*b*).

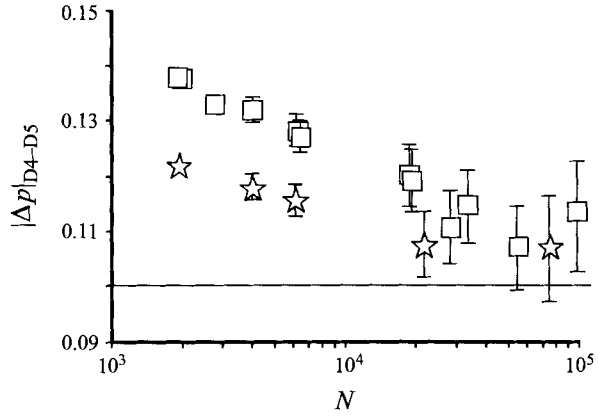

FIGURE 13. Pressure difference between D4 and D5 for a radial–toroidal flow (☆) and a toroidal-radial flow (□) as a function of N for $M = 7851$; $c = 0.052$ and $\Theta = 0°$. ——, Pressure drop predicted by the asymptotic model as $M, N \to \infty$.

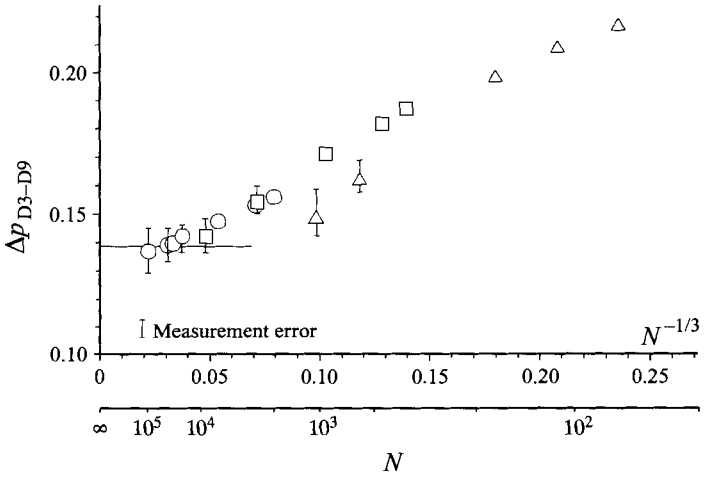

FIGURE 14. Pressure difference between D3 and D9 for various M and N; $c = 0.052$; $\Theta = 0°$; radial→toroidal flow. ○, $M = 7651$; □, $M = 3975$; △, $M = 1992$; ——, calculated pressure difference as $M, N \to \infty$.

The pressure difference between D5 and D9 becomes almost zero for large N. According to the sketch in figure 12(*b*), these two points correspond approximately to the same magnetic field line, so that equation (3.3) holds.

In figure 13 the pressure difference between the locations D4 and D5 is shown as a function of N for both flow directions. Similar to the wall potential measurements on the sidewalls near the bend, see figure 10, a clear dependence of the pressure drop on the flow direction exists. The pressure difference also depends significantly on N and diminishes as N increases. The pressure differences measured for a toroidal→radial flow are higher than those for a radial→toroidal flow, supporting the previously discussed hypothesis about the separation zone. With increasing N the measured values tend to the theoretical ones.

Finally the total pressure drop in the 90° bend between D3 and D9 is investigated. In figure 14 this pressure drop is shown as a function of N for various M in a

radial → toroidal flow. At high interaction parameters the measured values agree rather well with the ones calculated with asymptotic model. At low M and N however, the pressure drop is significantly higher than in the inertialess limit.

A fitting procedure based on the minimum of the error squared for the measured data leads to the following relation according to equation (5.3):

$$\Delta p_{D3\text{-}D9} = 0.135 + 0.406\, N^{-0.337} + 0.0939\, M^{-0.565}. \tag{5.4}$$

The first constant 0.135 corresponds with an accuracy of 3.5 % to the theoretical value. The exponents determined are very close to those predicted above.

5.2. *Sensitivity to magnetic field inclinations*

An important parameter in MHD flows is the orientation of the magnetic field with respect to the bend geometry. Depending on the field orientation with respect to the toroidal duct completely different flow patterns, velocity profiles and pressure drops can establish.

5.2.1. *Phenomenology of small field inclinations*

Figure 15 shows a bend with a negative and figure 16 a bend with a positive magnetic field inclination angle Θ. For simplicity inclinations of $\Theta < 0°$ are called forward bends, inclinations of $\Theta > 0°$ are called backward bends, according to the terminology introduced by Moon & Walker (1990) and Moon *et al.* (1991). In a backward bend the internal layer detaches from the second wall, and is able to carry a significant portion of the volume flux. In a forward bend two internal layers appear, which cross the bend's inner and outer corners. These layers are unable to carry any significant volume flux. An essential difference between flows in bends with $\Theta = 0°$ and those with $\Theta \neq 0°$ is that in the latter both the fully developed and three-dimensional pressure drop are not zero in both the radial and the toroidal ducts. Further features of flows with $\Theta \neq 0°$ can be found in a detailed discussion by Moon *et al.* (1991).

5.2.2. *Experimental results for small field inclinations*

(*a*) *Potential measurements*

Consider first the forward bend with $\Theta = -5°$ with a radial–toroidal flow. In figure 15 the wall potentials on the Hartmann walls at several positions are shown for different values of N. At line A nearly the same potential distribution as for $\Theta = 0°$ is obtained. As the flow approaches the internal layer from A over C to E the potential on the Hartmann wall decreases continuously. No influence of N can be detected, even at the transition to the sidewall at $z = -1$. The agreement of the experimental and numerical data at the positions H, I and J is good. However, near the outer corner at H and $z = -1$ a weak dependence of the potential on the interaction parameter appears, which increases a little up to position I. The absolute value of the measured potential is slightly higher than the calculated one. This may indicate that due to inertia forces more fluid in the cores C2 and C3 is pushed normal to the magnetic field at positions H and I than predicted by the asymptotic model, inducing a higher potential there.

To perform measurements for the inclination angle $\Theta = -5°$ the symmetry axis of the test section was rotated. Therefore the line P was located near the coils and experienced a radial magnetic field of 0.16 Tesla, which explains the discrepancies between prediction and experiment for this line.

In the backward bend for $\Theta = 15°$ a similar potential distribution on the radial duct

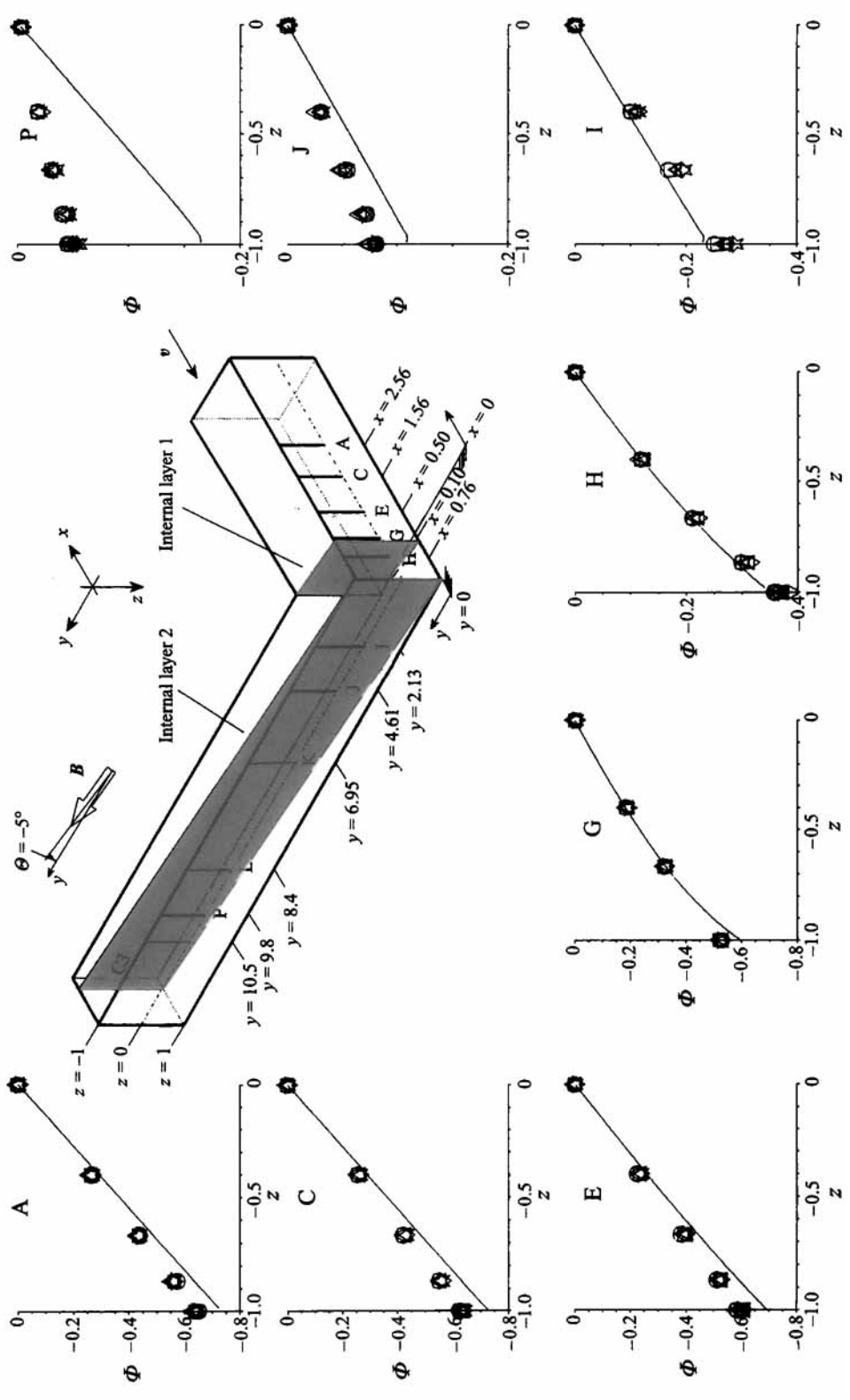

FIGURE 15. Wall potentials at lines A, C, , G, H, I, and P for different N; $M = 8125$; $c = 0.052$, $\Theta = -5°$; radial → toroidal flow. ○, $N = 30720$; □, $N = 20490$; △, $N = 5912$; ◇, $N = 3711$; ☆, $N = 1863$; ——, calculated potential distribution (M, $N \to \infty$).

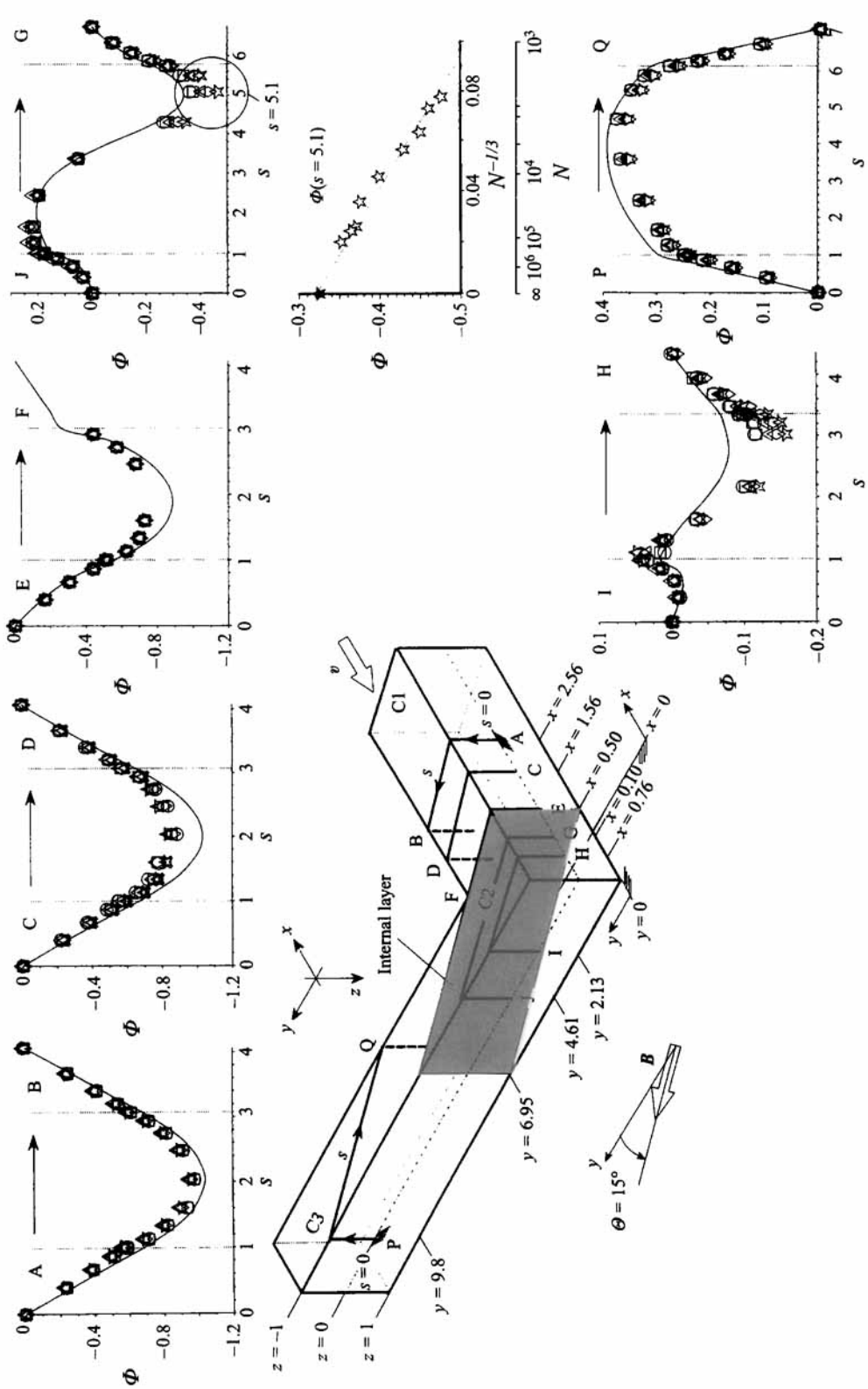

FIGURE 16. Wall potentials along the lines A→B, C→D, E→F, J→G, I→H and P→Q for different N as a function of s; $M = 8125$; $\epsilon = 0.052$, $\Theta = 15°$; radial→toroidal flow. ○, $N = 121\,300$; □, $N = 94\,910$; △, $N = 11\,000$; ◇, $N = 6867$; ☆, $N = 2143$; ——, calculated potential distribution (M, $N \to \infty$). The sidewall potential at the position $s = 5.1$ at the line J→G is also shown as a function of $N^{-1/3}$. The filled symbol in this graph indicates the calculated values for M, $N \to \infty$.

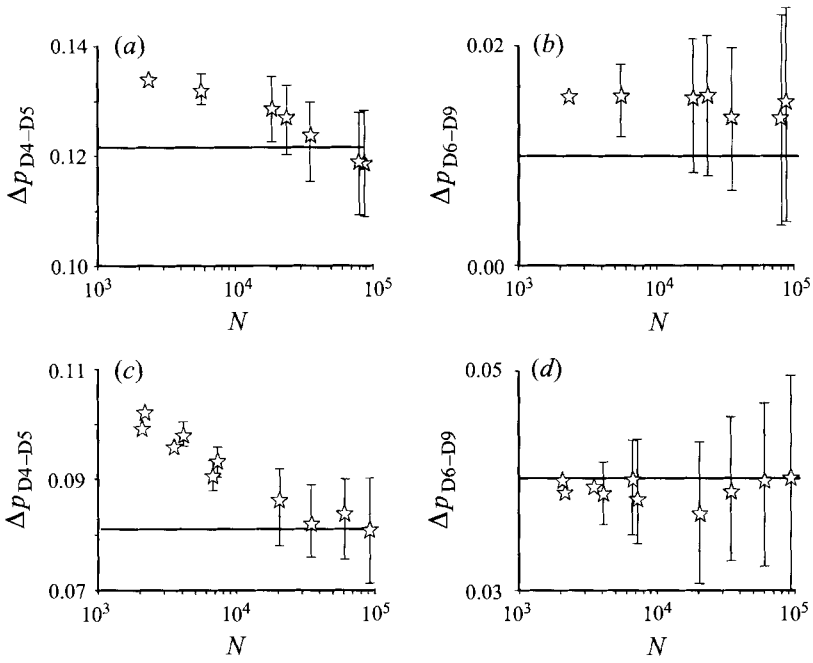

FIGURE 17. Pressure differences in a radial–toroidal flow at $M = 7785$; $c = 0.052$ as functions of N compared with the asymptotic values for M, $N \to \infty$ (——). (a, b) Forward elbow ($\Theta = -5°$); (c, d) backward elbow ($\Theta = 15°$).

surface is obtained as in the previously discussed cases. In figure 16 the measured potentials along different lines from A → B to P → Q are shown as a function of the coordinate s, which measures the distance along the perimeter of characteristic cross-sections aligned with the magnetic field, see the schematics in figure 16. In the inertialess model a large amount of fluid flows through the internal layer directly from the core C1 towards core C3, bypassing core C2. As a result the velocity and the potential in region C2 is small. Additionally in C2 the induced potential reverses its sign due to $\boldsymbol{v} \times \boldsymbol{B}$.

In the experiment more fluid will be transported through the internal layer into region C2 than the theory predicts because of inertia effects. Hence, more fluid flows in C2 inducing higher absolute values of the potential than predicted by the model. The absolute value of the potential increases with decreasing interaction parameter both on the Hartmann walls and on the sidewalls. The inertial part of the potential on the sidewalls increases proportionally to $N^{-1/3}$. This dependency of the potential on $N^{-1/3}$ is also shown in figure 16 for the characteristic point at $s = 5.1$ on the traverse J → G. With increasing interaction parameter the experimental data tend to those obtained by the asymptotic model. In extended measurements up to $N = 1.2 \times 10^5$ the inertialess value for the sidewall potential could not be completely reached. Inertia effects on the sidewall potential are clearly more manifested than in the case $\Theta = 0°$ (compare with figure 10). In region C3 the strong dependence of the potentials on N diminishes and at the line P → Q the potential shows a distribution which is qualitatively and quantitatively the same as predicted by the asymptotic model.

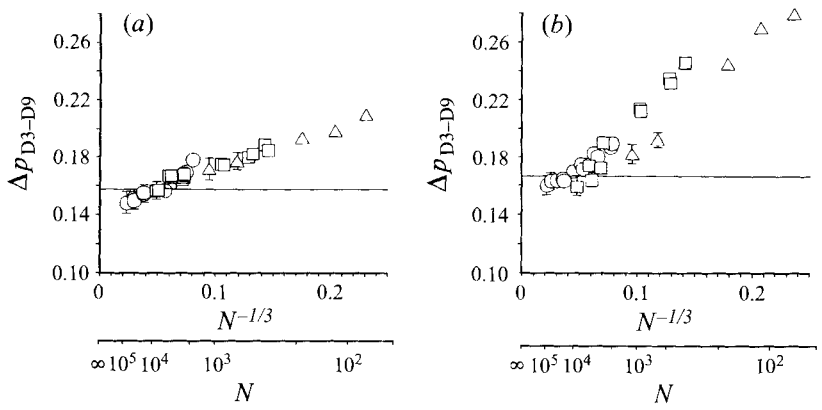

FIGURE 18. Pressure difference in a radial–toroidal flow between D3 and D9 at $c = 0.052$ as a function of N and M compared with the asymptotic values for M, $N \to \infty$ (——). (*a*) Forward elbow with $\Theta = -5°$; (*b*) backward elbow with $\Theta = 15°$. △, $M = 1952$; □, $M = 4175$; ○, $M = 7766$.

(*b*) *Pressure measurements*

In figure 17(*a–d*) the pressure differences between D4 and D5 as well as between D6 and D9 are shown for the inclinations $\Theta = 15°$ and $\Theta = -5°$. The dependence of the pressure drop on inertia effects in the vicinity of the bend can be clearly observed. With increasing N the pressure drop tends to the asymptotic value for both field inclinations, see figure 17(*a*, *c*). The dependence of the pressure drop on inertia is greater for the backward bend than for the forward bend because the internal layer plays a more important role in this case. In the toroidal duct between points D6 and D9 for both field inclinations no significant influence of inertia on the flow could be found, see figure 17(*b*, *d*). For the inclination angle $\Theta = 15°$ the agreement of calculated and measured values is quite good. In the forward bend the measured values are a little higher than the calculated ones. The pressure difference between D6 and D9 caused by the radial field components near the coils was estimated to be 0.01. This corresponds to the deviation from the theoretical value, which assumes a homogeneous uniform solenoidal magnetic field.

Let us discuss the total bend pressure drop between D3 and D9, which is shown in figure 18 as a function of N for various M and for $\Theta = -5°$, $+15°$. At high M and N the pressure drop tends to the asymptotic value in both cases. The pressure drop due to inertia $\Delta p_{3D,N}$ for both the forward and backward bends scales with $N^{-1/3}$, the same dependency as for $\Theta = 0°$.

For the backward bend a regression of the experimental data based on a least-squares fit and the correlation 5.3 provides ($\Theta = 15°$) the following relationship:

$$\Delta p_{D3-D9} = 0.164 + 0.6N^{-0.334} + 0.02M^{-0.53}. \tag{5.5}$$

Here, the first constant corresponds to the theoretical value with an accuracy of 3.5%. The additional pressure drop due to the variation of the Hartmann number $\Delta p_{3D,M}$ is nearly proportional to $M^{-1/2}$ and is small compared to the contribution originating from inertia effects, which depend approximately on $N^{-1/3}$.

(*c*) *Measurements of the potential gradient within the liquid metal*

Local probe experiments have been conducted only for the inclination angle $\Theta = 15°$, because with the available measuring technique sufficiently high signals are only available for this inclination. The probe signals were recorded twice in every

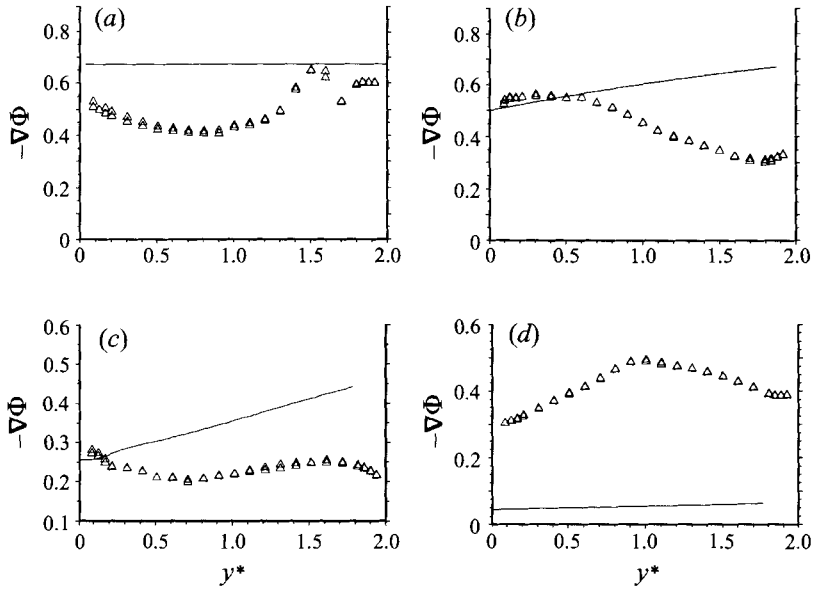

FIGURE 19. Potential gradients in the plane $z = 0$ for the stations S1 (*a*), S4 (*b*), S6 (*c*) and S7 (*d*) in the radial duct in the radial → toroidal flow for $M = 7.7 \times 10^3$; $N = 3.3 \times 10^4$; $\Theta = 15°$; and $c = 0.052$. ——, Calculated values as $M, N \to \infty$.

traverse. In the normalization of the potential gradient values the tip distance has been used as the characteristic geometrical length scale. The traversing coordinates y^* and x^* denote the dimensionless distance normal to the wall. In all measurements presented the sensing tips of the probe are facing the main flow, and the flow direction is radial → toroidal.

The potential gradient measurement at station S1 for $z = 0$ is shown in figure 19(*a*). Since the probe is inserted at the wall at $y = 0$ the wall there is locally electrically disturbed. The wakes arising from the prong and the locally lower electrical resistance lead to a potential decrease there, which may be explained by the effects described in the Appendix. This effect is not so pronounced at $y = 2$, because there the wall is not directly disturbed and therefore only an interaction of the wake with the wall exists. The agreement between predicted and measured gradients near the wall is within 20%. However, a remarkable difference with the prediction is found in the duct centre, where the potential decreases. We have no complete explanation for this effect, which may or may not indicate a reduced velocity in the duct centre due to the reduced potential.

Significant differences between model and measurements appear at S4 (figure 19*b*) and S6 (figure 19*c*). Near the wall at $y = 0$ the measured gradients are quantitatively the same as the ones predicted by the asymptotic theory. But in the interior of the duct the measured values are significantly lower (by up to 200%) and the shape of the potential gradient distributions is completely different from those predicted in the asymptotic model.

In the asymptotic model only the interaction of current and core pressure drives the fluid motion in the core. But the surface potentials in the $\Theta = 15°$ case show that inertia pushes the fluid towards the first wall. This is reflected in the surface potential measurements by a higher potential (see figure 16, line I → H). In the potential gradient measurements the same tendency has been found, as figure 19(*d*) at station S7 shows. The recorded data are many times higher than the calculated ones.

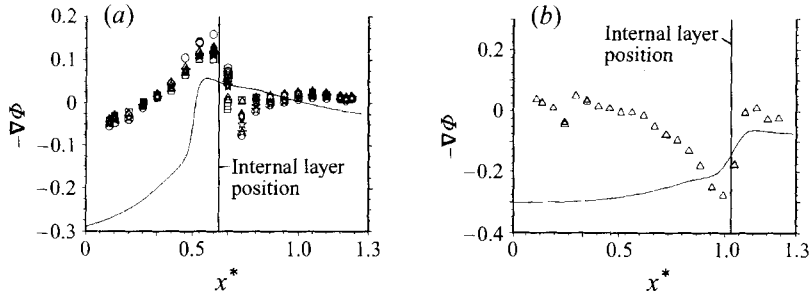

FIGURE 20. Potential gradients in the plan $z = 0$ for the stations S11 (*a*) and S14 (*b*) in the radial → toroidal flow for $M = 7.7 \times 10^2$; $c = 0.052$; and $\Theta = 15°$. □, $N = 3.34 \times 10^4$; △, $N = 2.29 \times 10^4$; ◇, $N = 7.04 \times 10^3$; ☆, $N = 3.5 \times 10^3$; ○, $N = 2 \times 10^3$; ——, calculated values as M, $N \to \infty$.

Further, in the toroidal duct the agreement between measured and calculated data gets worse. In figure 20(*a*) the dimensionless potential gradient at S11 is presented for different N. Particularly remarkable in this graph is the position $x = -0.66$, where the presence of the internal layer is clearly seen. Here the sign of the measured potential gradients changes within a rather small distance and the slope is higher than the model predictions by an order of magnitude. The strong dependence of the potential gradients on the interaction parameter at this special position is not so surprising. Also, at station S14 the biggest deviations between the model and the measurements have been found in the region of the internal layer, see figure 20(*b*). Nevertheless, the measured and the predicted potential gradient distributions there also differ not only quantitatively but also qualitatively.

We have no obvious explanation for the disagreement in the local measurements between the theory and the experiment. One of the possibilities is the negative effect of the probe that leads to the disturbance of the velocity profile (see the Appendix). This is supported by the fact that the experimental results tend only weakly to the asymptotic values as N increases. However we cannot exclude the possibility that this is just a pure inertial effect, and that the inertialess limit is far from being reached. In fact, as follows from the next section, these measurements were done for values of N close to the onset of time-dependent flow. This disagreement gives grounds for further work and for the development of another flow model (see Molokov *et al.* 1994).

5.3. *Stability considerations*

The asymptotic model discussed is based on the assumption of a laminar inertialess flow. Owing to the high-velocity jets in the parallel layers they may become unstable because of the inflection point in the velocity profiles and thus time-dependent flows may appear. Evidence of the instability of side layers in smooth three-dimensional flows has been provided by many authors. The most clear and detailed measurements have been performed by Reed & Picologlou (1989) investigating the flow in a straight rectangular duct into a fringing magnetic field. They found instabilities evolving from the side layers at a certain critical Reynolds number Re ($Re = M^2/N$). They state that the onset of instability is insensitive to the Hartmann number but the final state of the instability is strongly dependent on M. Related to this experiment Ting *et al.* (1991) performed a linear stability analysis for the side layers, which shows that the onset of turbulence is strongly dependent on M. The critical Reynolds number found in the analysis is $Re_{crit} = 313$ which is an order of magnitude smaller than in the experiments. Therefore, the questions about the onset of time-dependent flow, the type of instability developed and the layer thickness in which instabilities occur remain unanswered.

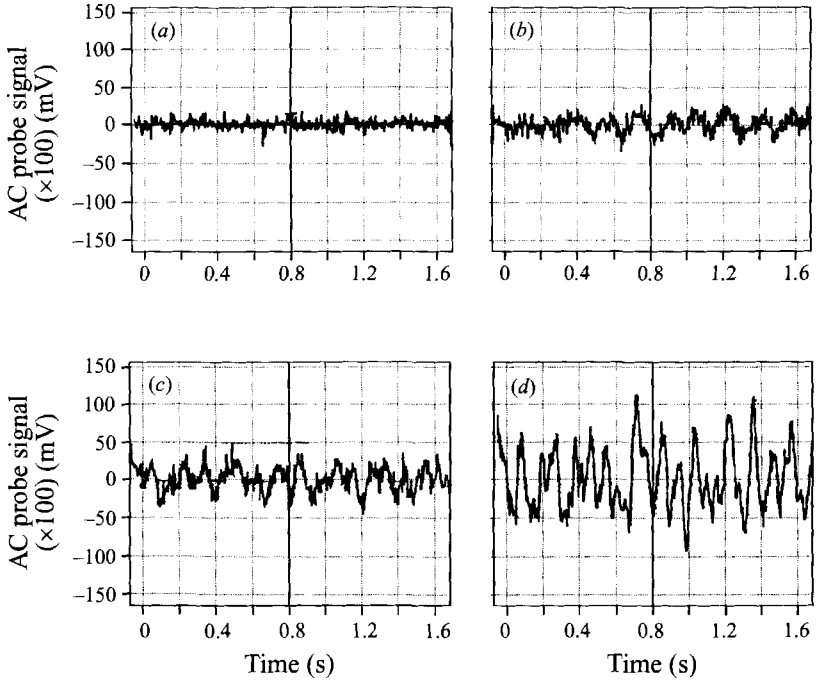

FIGURE 21. Time domain data for a local probe in the toroidal duct in the plane $y = 4.25$, $z = 0$ at the position $x = -0.6167$ in the radial→toroidal flow for $M = 7.8 \times 10^3$; $c = 0.052$; $\Theta = 15°$. (*a*) $N = 1.5 \times 10^4$; (*b*) $N = 1.5 \times 10^4$; (*c*) $N = 1.03 \times 10^3$; (*d*) $N = 4 \times 10^3$.

In order to detect the time-dependent flow phenomena which presumably occur near the inflection points of high-velocity jets like those in the side layers or the internal layers, traversable LEVI-probes were introduced in the bend at different locations. These measurements had three main aims:

(i) detection of the transition from laminar flow to time-dependent flow;

(ii) to find the spatial extent of domains with time-dependent flow;

(iii) to find the amplitude and frequency of the time-dependent signal.

The measurements were performed only for the inclination angle $\Theta = 15°$ and in planes $z = 0$ and $z = 0.92$. The Hartmann number was set to a constant value of $M = 7.8 \times 10^3$ and the interaction parameter was varied in the range $N = 2 \times 10^3$–3.5×10^4. This corresponds to Reynolds numbers $Re = 1.7 \times 10^3$–3×10^4. Based on the predictions of the asymptotic model a high-velocity jet associated with high shear stresses appears in the internal layer, which separates different flow domains, or in the side layers.

In the radial duct at the position S6 no time-dependent signals were observed throughout the investigated interaction parameter range. Even by crossing the internal layer location a fluctuating probe signal could not be observed.

In contrast to S6, in the toroidal branch at S11 highly localized time-dependent fluctuations were measured at two discrete positions of the traverse, namely $x = -0.6167$ and $x = -0.7167$ at $y = 4.25$. As expected oscillations are recorded near the left- and right-hand boundary of the shear layer, where the highest velocity gradients appear. The distance between these two locations is about twice the width of an inertial internal layer thickness $\sim N^{-1/3}$ for the investigated value of N, in accordance with the previous discussion.

In the next step at the same location the onset of time-dependent signals was

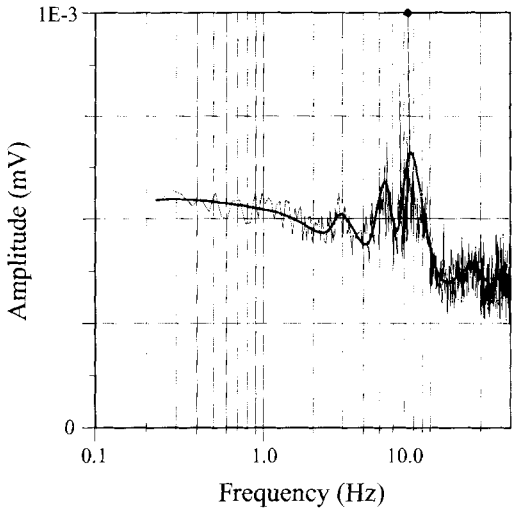

FIGURE 22. Fourier transform of the prbe signal at the position $x = -0.6167$ in the plane $y = 4.25$, $z = 0$ for $M = 7.8 \times 10^3$; $N = 4 \times 10^3$, $c = 0.052$; $\Theta = 15°$ for the radial→toroidal flow.

investigated at a fixed Hartmann number of $M = 7.8 \times 10^3$. The transition from steady to time-dependent signals was found at a critical interaction parameter of $N_{crit} = 10300$. Figure 21 (*a–d*) shows the time history for decreasing interaction parameters of $N = 3 \times 10^4 \rightarrow 4 \times 10^3$. It can be clearly seen in figures 21 (*c*) and 21 (*d*) that the signals exhibit characteristic frequencies. In figure 22 a Fourier transform of the time-dependent signal is shown for the position $x = -0.6167$ in the plane $y = 4.25$, $z = 0$ for $M = 7.8 \times 10^3$ and an interaction parameter of $N = 4 \times 10^3$. The transform shows that three frequencies are more preferred than others, namely 5.6, 6.8 and 7.2 Hz. The amplitude of the fluctuations is about 7.5 % to 9 % of the mean signal, which is smaller than Reed & Picologlou (1989) detected in their experiment.

The phenomenon has also been investigated at station S14 near the internal layer. The onset of time-dependent signals was found at the same critical interaction parameter with the same oscillation frequencies. In the whole toroidal duct only near the shear layers have highly localized oscillations been found, whereas in the rest of the flow domain the signals remained steady in time.

It should be noted in this context that the appearance of locally time-dependent flows at interaction parameters below N_{crit} does not lead to a measurable jump of the pressure drop in the duct.

6. Conclusions

In this article the MHD flow through sharp 90° bends of rectangular cross-section with electrically conducting walls is experimentally investigated, varying relevant parameters such as the Hartmann number M, the interaction parameter N and the inclination angle Θ of the magnetic field with respect to the bend. In particular, the fusion-relevant parameter range has been of interest, since for hydraulic components of fusion reactors the values of N are high, but often do not reach the values necessary for inertialess flow conditions, as assumed in the asymptotic models used for the design calculations.

Certain discrepancies between the asymptotic theory and the experiment, which have been discovered for both the wall potential and the pressure drop, may be partly

attributed to the following fact. For the theory to apply certain conditions have to be met, namely $c \gg M^{-1/2}$ for $N \gg M^{3/2}$, or $c \gg N^{-1/3}$ for $N \ll M^{3/2}$. These assumptions ensure that the electric current conducted by the parallel layers of whatever nature is negligible with respect to the wall current. None of these requirements has been fulfilled in the experiment. The other source of disagreement is the effect of the radial component of the magnetic field, not taken into account in the theory. This effect has been clearly demonstrated in several figures.

For the magnetic field inclination $\Theta = 0°$ the surface potentials on the Hartmann walls as well as on the first wall and the second wall revealed neither an influence of M nor of N. The data obtained agreed qualitatively and quantitatively well with the numerically calculated values using the asymptotic model. Based on this one can conclude that the MHD bend flow near the cores is inertialess and inviscid at high M ($M > 10^3$) and N ($N > 10^3$). However, at the sidewalls in the immediate vicinity of the bend, where high-velocity jets are expected, a dependence of the wall potential on inertia effects has been found. The wall potential there shows a dependence proportional to $N^{-1/3}$ for its inertial part. An extrapolation of the experimental data shows that the inertialess value calculated by the model assuming $N \gg M^{3/2}$, is reached approximately at $N \approx M^{3/2}$. At a distance of a few characteristic length from the bend the influence of inertia vanishes both on the wall potentials and on the pressure. The pressure measurements also show that at high Hartmann numbers ($M \approx 8 \times 10^3$) and high interaction parameters ($N \approx 10^5$) the agreement between model prediction and experiment is good. The deviations appearing are within the measurement accuracy or can be explained by the experimental conditions. However, the inertial part of the pressure drop $\Delta p_{3D,N}$, which is proportional to $N^{-1/3}$, can reach values which are comparable to the inertialess pressure drop. Together with the dependence of the sidewall potential on the interaction parameter N the $-1/3$ power law strongly suggests that inertial side layers are responsible for the inertial part of the pressure losses. In an inertial bend flow the flow direction influences the pressure drop. Owing to the nonlinear electromagnetic–inertia interaction the pressure drop in a toroidal–radial bend exhibits a higher pressure drop than a radial–toroidal flow; the dependence of $\Delta p_{3D,N}$ on N, however, remains proportional to $N^{-1/3}$ for both flow directions. The influence of the flow direction on the pressure drop is small compared to the total inertial pressure drop. Variations of the Hartmann number have a negligible influence on the pressure drop, which varies as $M^{-1/2}$, and on surface potential distribution in the investigated range of Hartmann numbers ($M > 10^3$).

By inclining the magnetic field with respect to the toroidal duct the bend flow exhibits different flow patterns, which are reflected both in wall potential and pressure distribution. For both inclination angles excellent agreement of the wall potential on the Hartmann walls, the first wall and the second wall has been found. An inclination of the magnetic field ($\Theta = 0°$) leads to a higher pressure drop compared to the aligned case ($\Theta = 0°$). The pressure drop in a backward bend ($\Theta > 0°$) is higher than in a forward bend ($\Theta < 0°$), since the flow direction changes with respect to the magnetic field and larger three-dimensional currents affecting the pressure drop circulate throughout the bend. In a backward bend the influence of inertia on the pressure drop is more clearly shown than in the $\Theta = 0°$ case or the $\Theta = -5°$ case; the inertial part of the pressure drop still depends on $N^{-1/3}$.

A detailed investigation of the inclination angle $\Theta = 15°$ showed that, like for $\Theta = 0°$, inertial side layers appear in the vicinity of the bend region. The inertial part of the sidewall potential there also scales with $N^{-1/3}$. The local potential gradient measurements within the fluid indicate that the bend flows remain laminar at a

Hartmann number of $M = 7.8 \times 10^3$ in all flow domains for interaction parameters $N > 10300$. By decreasing the interaction parameter below $N = 10300$ time-dependent oscillations were found near the internal layer location. The rest of the flow remains steady and laminar.

Significant differences have been detected between the theory and the experiment in local measurements of the potential gradients. Both the inertialess assumption of the theory and the measurement technique could be responsible for the disagreement. However, the present study clearly shows that inertia effects are important. The same conclusion has been reached by Reimann *et al.* (1994), who discovered unexpected velocity profiles in the toroidal duct of a U-bend for low values of the interaction parameter ($N \sim 10^2$–2×10^2) at Hartmann numbers $M \sim 2 \times 10^2$. The main conclusion is that the knowledge about MHD flows in strong magnetic fields is still insufficient. Considerably more effort is required in both theoretical and experimental research of MHD flows in complex geometries.

This work has been carried out as part of R. Stieglitz PhD research at the Forschungszentrum Karlsruhe. There, this work was performed in the framework of the Nuclear fusion project of the Forschungszentrum Karlsruhe and is supported by the European Union within the European Fusion Technology Program and the US Department of Energy. The authors are grateful to Dr B. F. Picologlou, Dr C. B. Reed, and Dr T. Q. Hua from the Argonne National Laboratory and Professor Dr U. Müller from the Forschungszentrum Karlsruhe for their help in planning, performing the experiments and many hours of constructive discussions interpreting the experimental results.

Appendix

A.1. *Measurement principle and experimental set-up*

The liquid metal electromagnetic velocimetry instrument (LEVI) is in principle a miniaturized electromagnetic flow meter measuring potential gradients. According to Ohm's law (equation (2.4)), the potential gradient becomes directly proportional to the velocity components perpendicular to the magnetic field, if electrical current are small. In duct flows with a wall conductance ratio $c \ll 1$ the local current density $\boldsymbol{j}$ can be neglected in most cases. In strongly three-dimensional flows like the bend flows three-dimensional currents may reach higher values so that direct conclusions about the velocity are not possible.

The LEVI-probes used in the experiment are traversable normal to the wall, have a stainless steel shaft of 3 mm in diameter and two sensing tips of 0.5 mm in diameter located in a plane $z = \text{constant}$. The stainless steel shaft of the prong is made electrically insulating by painting. Also the gold plated sensing wires were painted except for the tip. The distance between the tips is 1.97 mm. The measurements were carried out in the plane $z = 0$.

More details about LEVI probes can be found in Reed & Picologlou (1986).

A.2. *Some considerations on probe measurements in MHD flows*

In hydrodynamic flows around bodies boundary layers at the body surface develop due to the viscosity of the fluid. The form and thickness of the layers is determined by an equilibrium of inertia and viscosity. The influence of the body on the flow is mainly confined to a small area behind the body. For MHD flows in addition to these forces, electromagnetic forces play a significant role. They may be even dominant and favour

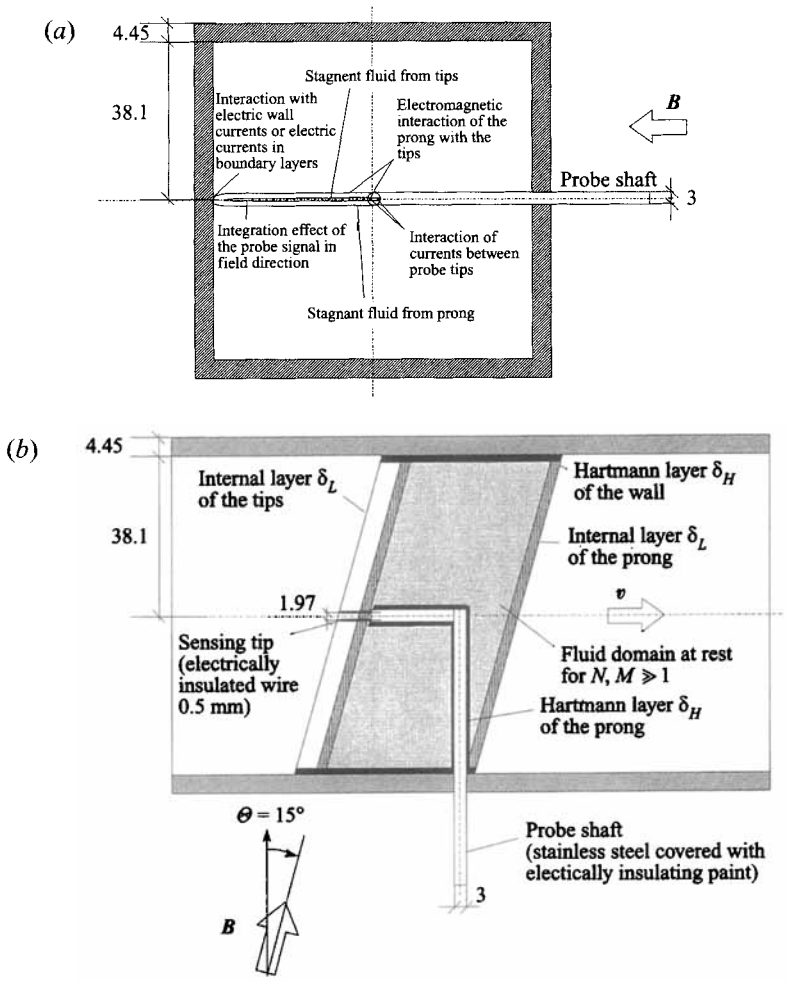

FIGURE 23. Sketch of the LEVI-probe inserted in the duct. Included in the graph are the possible electromagnetic interactions between the wall, the probe and the flow in a three-dimensional MHD-duct flow. (*a*) The front view of the radial duct; (*b*) a top view of the radial duct.

the development of a stagnant fluid area behind and in front of the body in the magnetic field direction. As for the discontinuous slope of a duct cross-section with respect to the magnetic field, also when inserting a probe in a MHD flow free shear layers (internal layers) appear separating different flow domains, see figure 23(*a*). The length scale of the stagnant fluid domain upstream and downstream is directly proportional to the Hartmann number of the body M_{body} (provided inertia effects are not dominant) and affects, as calculations of Kyrlidis, Brown & Walker (1990) have shown the flow in a quite large region.

Related to these flow phenomena that appear, several aspects of probe measurements in duct flows and the conclusions which one can draw from the data obtained are outlined. Putting an arbitrary body into a duct flow affects the flow structure in the duct and thereby leads to different signals than for an undisturbed flow. The probe shaft Hartmann number in the experiment is about $M_{probe} \approx 3 \times 10^2$, so that electromagnetic disturbances originating from the shaft influence the three-dimensional MHD flow over quite a large distance. The same holds for the sensing tip of the probe, for which the Hartmann number is about $M_{tip} \approx 50$.

Consider now a traversable probe consisting of a prong and two sensing tips within a duct extent, see figure 23(*b*). At high M the zones in which the flow is disturbed may reach the duct walls. This is probably the case in the present experiment. Electrical currents flowing in the wall can short-circuit through the zone from one duct wall to the other. As a result the global current path in the duct is changed and completely different flow patterns may be established compared to an undisturbed flow. This effect is most clearly seen for strongly three-dimensional flows.

If the shaft of the probe prong is electrically conducting, electrical currents induced in the liquid metal can enter the prong and reduce the potential difference between wall and fluid. This also leads to local changes of the flow structure. In probes in which the prong is non-unidirectional (probes which have a 90° bend) a shadowing of the sensing tips by the MHD wake of the prong may also occur leading to irregular measurement results.

The wakes arising from the sensing tips equalize the potential in the stagnant columns in the magnetic field direction. The measured potential gradients therefore represent some integral potential difference between the two columns in the flow. If the probe is near the wall, complex current paths between conducting walls, probe prong, sensing tips, different boundary and internal layers may appear, which lead to unpredictable current paths and thereby to misleading probe signals.

Besides these viscous–electromagnetic effects, inertial–electromagnetic effects may also change the flow pattern locally and globally. In the internal layers that appear, which separate the flow domains, shear stresses may occur, which lead to the production of quasi-two-dimensional vortices. There are several indications that these vortices may persist for quite a long distance, see Moreau (1990).

Generally the effects arising from these phenomena are small as long as the flow is two-dimensional or slightly three-dimensional as several experimentators have shown in the past, see e.g. Reed, Picologlou & Walker (1987). But as soon as three-dimensional currents play a significant role the electromagnetic influence of the probe has to be considered. The lack of an adequate theoretical background for the probe influence in a duct flow on the flow itself and therefore on the probe signal prevents clear analysis of the signals.

REFERENCES

BARLEON, L., BÜHLER, L., MACK, K.-J., MOLOKOV, S., STIEGLITZ, R., PICOLOGLOU, B. F., HUA, T. Q. & REED, C. B. 1992 Investigations of liquid metal flow through a right angle bend under fusion relevant conditions. *Proc. 17th Symp. on Fusion Technology* (*SOFT*), *Rome*, vol. 2, pp. 1276–1280. Elsevier.

BARLEON, L., BÜHLER, L., MACK, K.-J., STIEGLITZ, R., PICOLOGLOU, B. F., HUA, T. Q. & REED, C. B. 1993*a* Liquid metal flow through a right angle bend in a strong magnetic field. *Fusion Technol.* **21**(3) (2B), 2197–2203.

BARLEON, L., BÜHLER, L., MOLOKOV, S., STIEGLITZ, R., PICOLOGLOU, B. F., HUA, T. Q. & REED, C. B. 1993*b* Magnetohydrodynamic flow through a right angle bend. *Magnetohydrodynamics* **30**, 428–438.

BARLEON, L., CASAL, V. & LENHART, L. 1991 MHD-flow in liquid metal cooled blankets. *Fusion Engng Des.* **14**, 401–412.

BOCHENINSKII, V. P., TANANAEV, A. V. & YAKOVLEV, V. V. 1977 An experimental study of the flow of an electrically conducting liquid along curved tubes of circular cross-section in strong magnetic fields. *Magnetohydrodyn.* **14**, 431–435.

BÜHLER, L. 1993 Magnetohydrodynamische Strömungen flüssiger Metalle in allgemeinen dreidimensionalen Geometrien unter der Einwirkung starker, lokal variabler Magnetfelder. *Kernforschungszentrum Karlsruhe Rep.* 5095.

BÜHLER, L. 1995 Magnetohydrodynamic flows in arbitrary geometries in strong non-uniform magnetic fields – a numerical code for the design of fusion reactor blankets. *Fusion Technol.* **27**, 3–24.

GRINBERG, G. K., KAUDZE, M. Z. & LIELAUSIS, O. A. 1985 Local MHD resistances on a liquid sodium circuit with a super-conducting magnet. *Magnetohydrodyn.* **21**, 93–103.

HOLROYD, R. J. 1979 An experimental study of the effects of wall conductivity, non-uniform magnetic fields and variable area ducts on liquid metal flows at high Hartmann number. Part 1. Ducts with non-conducting walls. *J. Fluid Mech.* **93**, 603–630.

HOLROYD, R. J. 1980 An experimental study of the effects of wall conductivity, non-uniform magnetic fields and variable area ducts on liquid metal flows at high Hartmann number. Part 2. Ducts with conducting walls. *J. Fluid Mech.* **96**, 355–374.

HOLROYD, R. J. & HUNT, J. C. R. 1980 Theoretical and experimental studies of liquid metal flow in strong non-uniform magnetic fields in ducts and complex geometry. *Proc. 2nd Beer-Sheva Intl Seminar on MHD-Flows and Turbulence* (ed. H. Branover & A. Yakhat), pp. 23–43. Israel Universities Press.

HOLROYD, R. J. & MITCHELL, J. T. D. 1984 Liquid Lithium as a coolant for Tokamak Reactors. *Nuclear Engng Des./Fusion* **1**, 17–38.

HUA, T. Q. & WALKER, J. S. 1991 MHD considerations for poloidal-toroidal coolant ducts of self-cooled blankets. *Fusion Techn.* **19**, 951–960.

HUNT, J. C. R. 1965 Magnetohydrodynamic duct flow in rectangular ducts. *J. Fluid Mech.* **21**, 577–590.

HUNT, J. C. R. & HOLROYD, R. J. 1977 Applications on laboratory and theoretical MHD duct flow studies in fusion reactor technology. *UKEA-CLM-R*169. Culham Laboratory; Abingdon, Oxfordshire.

HUNT, J. C. R. & LEIBOVICH, S. 1967 Magnetohydrodynamic duct flow in channels of variable cross-section with strong transverse magnetic field. *J. Fluid Mech.* **28**, 241–260.

KULIKOVSKII, A. G. 1968 On slow steady flows of conductive fluid with high Hartmann number. *Fluid Dyn.* **3**, 1–5.

KYRLIDIS, A., BROWN, R. A. & WALKER, J. S. 1990 Creeping flow of a conducting fluid past axis-symmetric bodies in the presence of an aligned magnetic field. *Phys. Fluids* A **2**, 2230–2239.

MALANG, S., ARHEIDT, K., BARLEON, L., BORGSTEDT, H.-U., CASAL, V., FISCHER, U., LINK, W., REIMANN, J. & RUST, K. 1988 Self-cooled liquid-metal blanket concept. *Fusion Technol.* **14**, 1343–1356.

MOLOKOV, S. 1993 Fully developed liquid-metal flow in multiple rectangular ducts in a strong uniform magnetic field. *Eur. J. Mech./B. Fluids* **12**, 769–787.

MOKOKOV, S. & BÜHLER, L. 1994 Liquid metal flow in a U-bend in a strong uniform magnetic field. *J. Fluid Mech.* **267**, 325–352.

MOLOKOV, S. & BÜHLER, L. 1995 Asymptotic analysis of magnetohydrodynamic flows in bends. *Z. Angew. Math. Mech.* **75**, 345–346.

MOLOKOV, S., BÜHLER, L. & STIEGLITZ, R. 1994 Asymptotic structure of magnetohydrodynamic flows in bends. *Proc. 2nd Intl Conf. on Energy Transfer in Magnetohydrodynamic Flows.* Aussois, France, 26–30 Sept., 1994, pp. 473–484.

MOON, T. J., HUA, T. Q. & WALKER, J. S. 1991 Liquid metal flow in a backward elbow in the plane of a strong magnetic field. *J. Fluid Mech.* **227**, 273–292.

MOON, T. J. & WALKER, J. S. 1990 Liquid metal flow through a sharp elbow in the plane of a strong magnetic field. *J. Fluid Mech.* **213**, 397–418.

MOREAU, R. 1990 *Magnetohydrodynamics*, pp. 272–304, 165–197. Kluwer.

O'DONELL, J. O., PAPANIKOLAOU, P. G. & REED, C. B. 1989 The thermophysical transport properties of eutectic NaK near room temperature. *Argonne National Laboratory/Fusion Power Program* rep. *TM*-237.

REED, C. B. & PICOLOGLOU, B. F. 1986 Techniques for mesurements of velocity in liquid metal MHD-flows. *7th Top. Meeting on Fusion Technology, Nevada.*

REED, C. B. & PICOLOGLOU, B. F. 1989 Side wall flow instabilities in a liquid metal MHD-flow under blanket relevant conditions. *Fusion Technol.* **15**, 705–715.

REED, C. B., PICOLOGLOU, B. F. & WALKER, J. S. 1987 ALEX-Results – A comparison of

measurements from a round and a rectangular duct with 3D-code predictions. *IEEE* 87CH2507-2, vol. 2, pp. 1267–1270.

REIMANN, J., BUCENIEKS, I., DEMENTIEV, S., FLEROV, A., MOLOKOV, S. & PLATNIEKS, I. 1994 MHD-velocity distributions in U-bends partially parallel to the magnetic field. *Proc. 2nd Int. Conf. on Energy Transfer in Magnetohydrodynamic Flows, Aussois, France, 26th–30th Sept., 1994*, pp. 391–402.

STIEGLITZ, R. 1994 Magnetohydrodynamische Strömungen in Ein- und Mehrkanalumlenkungen (in German). University of Karlsruhe, PhD thesis.

TILLACK, M. S. 1990 Magnetohydrodynamic flow in rectangular ducts-design equations for pressure drop and flow quantity. *UCLA-FNT*-41.

TING, A. L., WALKER, J. S., MOON, T. J., REED, C. B. & PICOLOGLOU, B. F. 1991 Linear stability analysis for high velocity boundary layers in liquid metal magnetohydrodynamics. *Intl J. Engng Sci.* **29**, 939–948.

WALKER, J. S. 1981 Magnetohydrodynamic duct flows in rectanguar ducts with thin conducting walls, Part I. *J. Mèc.* **20**, 79–112.

WALKER, J. S., LUDFORD, G. S. S. & HUNT, J. C. R. 1972 Three-dimensional MHD duct flows with strong transverse magnetic fields. Part 3. Variable rectangular ducts with insulating walls. *J. Fluid Mech.* **56**, 121–141.